Journal of Manufacturing Processes 103 (2023) 413–429

Contents lists available at ScienceDirect

Journal of Manufacturing Processes

journal homepage: www.elsevier.com/locate/manpro

Review

Laser powder bed additive manufacturing: A review on the four drivers for an online control

Francesco Lupi [a,*], Alessio Pacini [b], Michele Lanzetta [b]

[a] Department of Information Engineering, 56122 Pisa, Italy
[b] Department of Civil and Industrial Engineering, 56122 Pisa, Italy

ARTICLE INFO

Keywords:
AM online control
L-PBF
Metal additive manufacturing
Closed-loop control
In-situ monitoring
Machine learning

ABSTRACT

Online control of Additive Manufacturing (AM) processes appears to be the next challenge in the transition toward Industry 4.0 (I4.0). Although many efforts have been dedicated by industry and research in the last decades, there remains substantial room for improvement. Additionally, the existing scientific literature lacks a wide-ranging identification and classification of the primary drivers that enable online control of AM processes. This article focuses on online control of one of the most industrially widespread AM processes: metal Laser Powder Bed Fusion (L-PBF), with particular emphasis on two subcategories, namely Selective Laser Sintering (SLS) and Selective Laser Melting (SLM). Through a systematic literature review, this article initially identified over 200 manuscripts. The search was conducted utilizing a defined research query within the Scopus database, double checked on Scholar. The results were refined through multiple phases of inclusion/exclusion criteria, culminating in the selection of 95 pertinent papers. This article aims to provide a systematic and comprehensive review of four identified drivers i) Online controllable input parameters, ii) Online observable output signatures, iii) Online sensing techniques, iv) Online feedback strategies, adopted from the general Deming control loop Plan-Do-Check-Act (PDCA). Ultimately, this article delves into the challenges and prospects inherent in the online control of metal L-PBF.

1. Introduction

Born almost forty years ago, Additive Manufacturing (AM) emerges as one of the most promising non-conventional manufacturing processes and has since become a key enabling technology in the current Industry 4.0 (I4.0) revolution [1,2]. AM allows for a higher degree of freedom in shaping compared to traditional manufacturing methods, but it does come with some trade-offs, such as limited mechanical properties and process productivity [3]. To date, the aerospace, defense, and biomedical industries have made the most significant investments in this sector, driven by the demand for highly customized parts, followed by other sectors like tooling, jewelry, and automotive [4]. Around 2018, the hype surrounding AM subsided in the mass media, but interest in research and commercial applications has never been higher [5,6]. Notably, thousands of companies are now leveraging AM, leading to a remarkable industry expansion of 7.5 % that resulted in nearly $12.8 billion in revenue in 2020 [7,8]. Within this dynamic landscape, this article focuses on one specific class of AM technologies, namely Powder Bed Fusion (PBF) [9], as depicted by the dotted box in Fig. 1.

PBF was among the earliest and has remained one of the most versatile AM processes, catering to polymers and metals as well as ceramics, composites, and biomaterials [10]. Among several thermal sources, laser, and electron beams, respectively referred to as Laser Powder Bed Fusion (L-PBF) and Electron Beam Powder Bed Fusion (E-PBF), are the most historically acknowledged techniques. The third type of thermal source which has recently entered the market uses Infra-Red (IR) lamps [11]. Table 1 provides a brief overview of the four subclasses of PBF, categorized based on the thermal source, as highlighted in Fig. 1.

The focus of this article, indicated by the blue/shaded labels in Fig. 1 and Table 1, lies on L-PBF (i.e., SLS and SLM), with particular emphasis on metal powders due to their increasing significance [12,13].

Online process control for metal L-PBF is still in its development stages [14]. Despite the sophistication of AM machines and digital twin capabilities, the process is often operated as an open loop, with users manually tuning process parameters based on post-process characterization and analysis [15,16]. While some authors and vendors have proposed actual online control strategies, they are limited, primarily relying on simple alarms or process blocking upon defect detection

* Corresponding author.
E-mail address: francesco.lupi@phd.unipi.it (F. Lupi).

https://doi.org/10.1016/j.jmapro.2023.08.022
Received 1 August 2022; Received in revised form 31 July 2023; Accepted 6 August 2023
Available online 8 September 2023

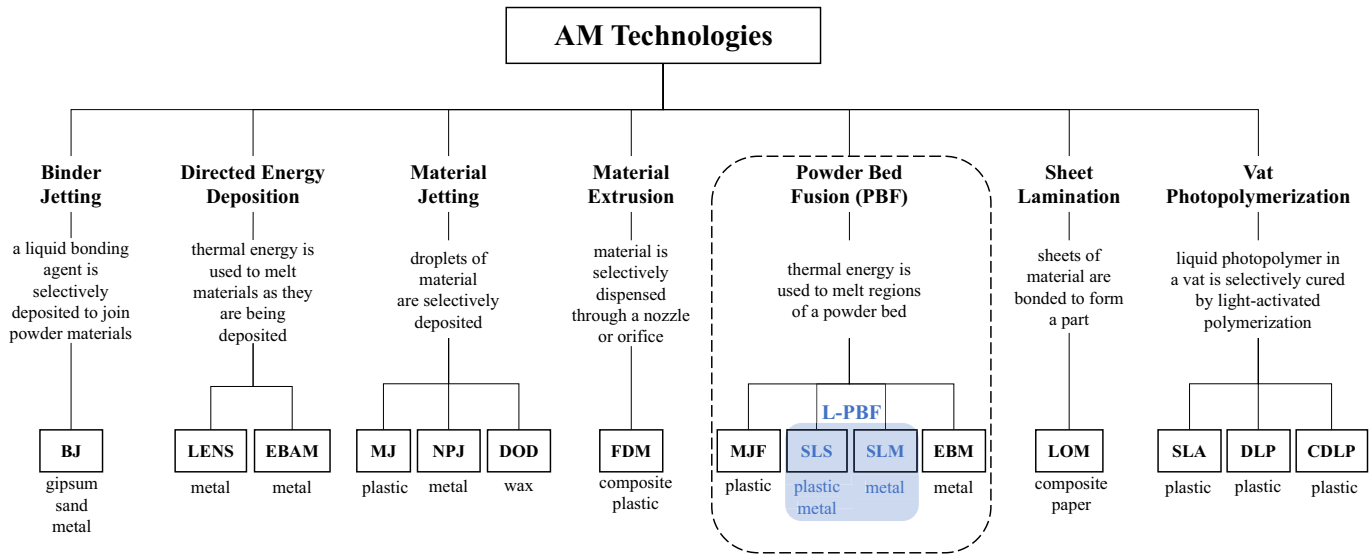

Fig. 1. The AM technologies classes, descriptions, subclasses, and primary materials from [9]. In blue/shaded the two subclasses in-scope of the present article. For each subclass, the extended name is provided from left to right. Binder Jetting (BJ), Laser Engineering Net Shape (LENS), Electron Beam Additive Manufacturing (EBAM), Material Jetting (MJ), Nano Particle Jetting (NPJ), Drop On Demand (DOD), Fused Deposition Modeling (FDM), Multi Jet Fusion (MJF), Selective Laser Sintering (SLS), Selective Laser Melting (SLM), Electron Beam Melting (EBM), Laminated Object Manufacturing (LOM), Stereolithography (SLA), Digital Light Processing (DLP), Continuous Digital Light Processing (CDLP). (For interpretation of the references to color in this figure legend, the reader is referred to the web version of this article).

[4,17,18]. This article aims to investigate current gaps of online control by reviewing the state of the art of four major process drivers inspired from the Deming cycle [19] loop control (Fig. 2) and following the review protocol proposed by [20].

As depicted by Fig. 2, online controllable input parameters are the starting point. These parameters are planned (i.e., P-Plan) in advance and then actuated during the production process (i.e., D-Do), thereby generating process signatures. The next step involves monitoring these online observable output signatures using appropriate in-situ sensors (i.e., C-Check). Subsequently, the sensors provide a stream of data used to adjust the input parameters in accordance with the feedback strategies (i.e., A-Act).

Our article builds upon and extends the reviews conducted by [4,17,21–24], adopting aligned standard terminology, considering more recent papers, and following the structured approach in reviewing scientific articles for each of the four drivers presented in Fig. 2. Our overarching objective is to provide readers with a comprehensive and clear understanding of the complexities surrounding online control of metal L-PBF processes, tackling interdisciplinarity topics from a holistic perspective.

The remainder of the article is organized as follows and is visually presented in Fig. 3. The scope and Research Questions (RQs) have been defined as input for the review process. The subsequent article sections have been planned and implemented to ensure a logical and coherent flow (Fig. 3, center), and the related contributions have been presented to address the initial RQs within the scope of this article (Fig. 3, right side).

While Section 1 aims identifying the first contribution of this article (i.e., adopting the Deming cycle carefully customized to formalize the online control of L-PBF processes), Section 2 introduces the metal L-PBF process, providing the context of this work. Section 3 details the structured procedure adopted to carry out the literature review on the four drivers, answering the first RQ1: *what aspects do we aim to examine in the literature?* Section 4 reports and summarizes the state of the art on the four drivers, based on the final set of 95 selected papers filtered from an initial list of over 200 Scopus indexed papers. This section offers a detailed account of the literature, addressing RQ2: *what are the primary approaches found in the literature?* In Section 5, we provide a concise overview and takeaways from the main aspects of the four drivers, along with their current level of maturity, to answer RQ3: *what are the key findings from the literature*? Section 6 focuses on the future directions and challenges concerning data collection, management, and processing for metal L-PBF online control, addressing RQ4: *what are the main future challenges?* Although the focus of this article is on metal L-PBF, the readers can readily apply the methodology used in this article, including the four drivers, to other specific AM techniques and various materials.

2. Metal L-PBF process overview

In this section, we present a comprehensive overview of metal L-PBF to provide context for the current study. Fig. 4 summarizes the general AM process (depicted in white), with the addition of an online closed

Table 1
The four PBF processes, short description, thermal source and required power. In blue the process in-scope of the present article.

PBF subclasses	Short description	Thermal source	Required power
MJF	In the MJF process, IR lamps pass over the surface and distribute the heat on previously jetted material to selectively melt plastic powder particles.	IR lamps	Low
SLS	SLS is a specific type of L-PBF that uses lasers to bind powder by only melting the particles' surface. It usually requires further processing (e.g., infiltration) to make the component fully dense.	Laser beam	Low
SLM	Also known as Direct Metal Laser Sintering (DMLS) or Direct Metal Laser Melting (DMLM). As opposed to SLS, SLM uses high power laser beams to melt the powder particles, fusing to the previous layers to produce fully dense parts.	Laser beam	High
EBM	The EBM process deals with high power energy similarly to SLM, but it uses electron beams instead of the laser-based approach. This latter process is mainly used for metals.	Electron beam	High

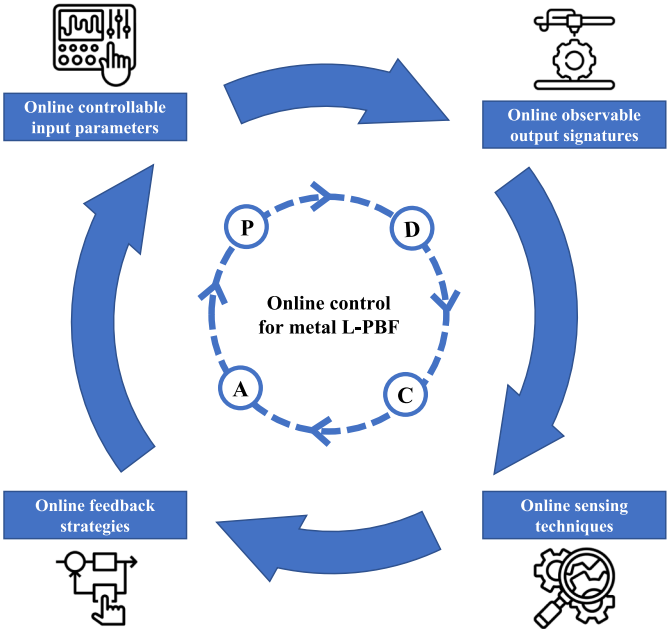

Fig. 2. Graphical outline of the article. The four drivers are highlighted in the boxes. Each box has been labeled via the initials of Deming's control loop steps (P-Plan, D-Do, C-Check, A-Act) [19].

control loop (shown in green) and Statistical Process Control (SPC)/ monitoring (shown in orange). The high-level flow diagram illustrates the different phases of the process (represented by solid boxes) and the outputs (represented by dotted boxes). Solid arrows indicate the logical flow of the process, while dotted arrows represent the information flow.

Control-limit detection in SPC are widely recognized as the industry standard for in-situ detection and control of L-PBF processes [25]. Traditional SPC control charts, pioneered by Shewhart, enable the establishment and maintenance of statistical control over critical outputs in complex manufacturing and process environments. By analyzing samples and assessing quality characteristics, control charts help identify changes in process levels and detect non-random patterns that indicate the need for intervention. An out-of-control situation occurs when special causes, in addition to common-cause variations inherent in the process, begin to influence the process output. Control limits (i.e., upper, and lower), calculated using different methods, serve as thresholds for sample data and prompt necessary actions such as process adjustment or investigation when measures fall outside these limits. Despite the potential demonstrated by using process limits as a viable and practical method for detecting undesirable conditions, the focus of control charts is on identifying abnormal process conditions rather than identifying individual defects or implementing real time process corrections. Therefore, the alarms provided by the recorded data are not sufficient to manage the inevitable and unpredictable variations of the process conditions and to ensure parts' consistency. Additionally, these detection limits are often hardcoded and derived from experimental processes, operator experience, or simulations, rather than being learned from data, as is the case with new trending Machine Learning (ML) techniques [26]. For this reason, an advanced control strategy (Fig. 4, green) with closed online control loop (red enclosed area) is needed [27]. In the following Sections 2.1 and 2.2, a brief description of offline control loops and general AM activities is reported. This introduction aims to provide a comprehensive understanding of the manufacturing process behind the four drivers reviewed for closed online control loop.

2.1. *Requirements, constrains and knowledge management*

During the part design stage (Fig. 4, white, left-side), a virtual 3-Dimensional (3D) model of the geometry intended for manufacturing is created using Computer-Aided-Design (CAD) software [28] or derived from scan data of an existing physical object [29]. Subsequently, the 3D model is converted into a Standard Tessellation Language (STL) file format, which describes the surface of the object using triangular facets

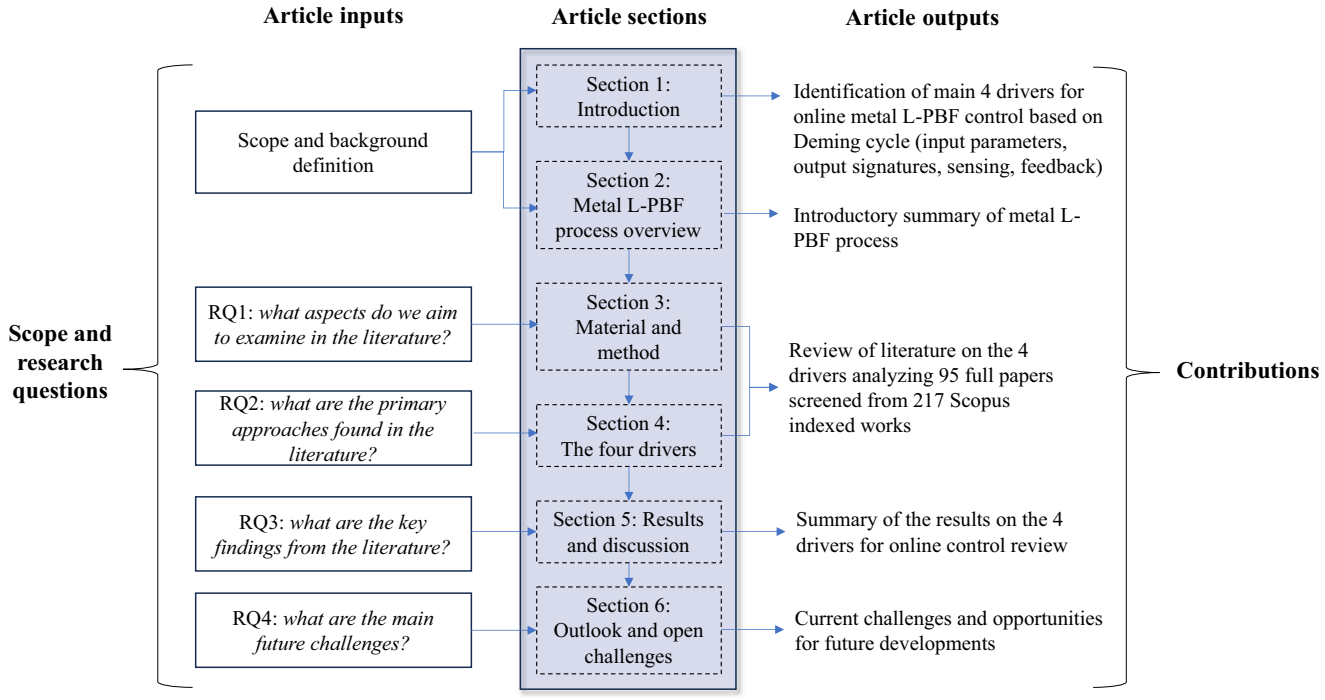

Fig. 3. The article structure according to the scope and RQs as input, article sections (highlighted in blue) and article contributions as output, all focused on the state of the art of metal L-PBF.

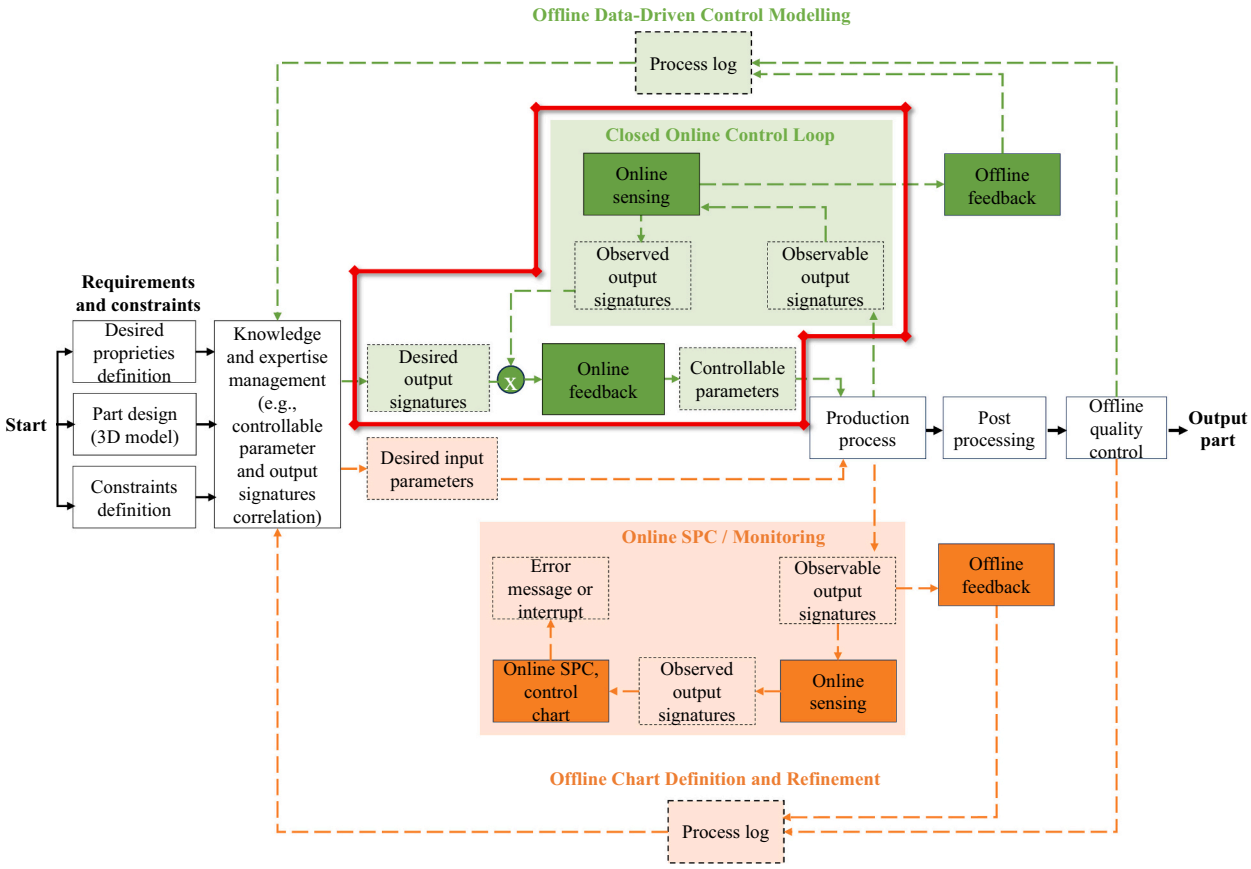

Fig. 4. AM process flow diagram with general activities in white. Closed online control loop in green and industrial standards (with SPC) in orange. The green red enclosed area represents the core of the current article. Offline data-driven control modeling represents the refinement and tuning loop of the controller, involving the development of relationships between controllable parameters and observable signatures through a data-driven approach. The orange area represents the core of the SPC and monitoring process. Offline chart definition and refinement represents the offline tuning for SPC, including tasks such as limits definition and refinement. The offline loop is adopted for the modeling of the process through a data-driven approach, focusing on developing relationships between controllable parameters and requirements/constraints. (For interpretation of the references to color in this figure, the reader is referred to the web version of this article.)

[30]. This mathematical separation of the 3D volumetric model into slices generates a machine-readable G-Code that contains all instructions for the motors and other machine components, serving as additional input parameters [31,32].

As shown in Fig. 4 (white, right-side), the production process requires setting up controllable input parameters for the AM machine. These parameters can be categorized into two main groups: i) predefined parameters that remain constant throughout the entire process and ii) online controllable input parameters. Predefined input parameters include: laser type (e.g., CO_2, Nd: YAG, laser fiber) [33–35], laser operating mode (i.e., continuous, pulsed) [36], laser beam quality factor [37]; powder properties (e.g., material, size, thermophysical and flowability properties [38,39]); inert gas type (e.g., argon, nitrogen) [40]; and recoating mechanism (e.g., stiff scraper, soft squeegee, roller) [41]. Detailed information about online controllable input parameters (i.e., one of the four drivers reviewed in this article) will be provided in Section 4. Through proper knowledge management and offline loops (Fig. 4, external loops), experimental correlation of input parameters and output signatures can be derived. These correlations are utilized in both SPC and closed control approaches to achieve desired properties of the manufactured part, typically through experimental data-driven approach (e.g., Design of Experiments DOE) [44]. SPC acts as a safeguard by halting production if process signatures deviate beyond acceptable limits. On the other hand, the closed control approach goes beyond mere monitoring when an issue arises. It involves a feedback loop that dynamically modifies specific controllable input parameters during the manufacturing process [42]. This adjustment is done in real time to align the output signatures with the desired ones.

The external loops can be associated also to the “long run”, or “systemic” corrective actions promoted by ISO 9001 continuous improvement approach, which relies on developing process knowledge through objective evidence (i.e., process logs) [43]. However, the development of these offline cycles is beyond the scope of this article, and the desired output signatures as well as related input parameters are assumed known in the following sections.

2.2. Production process, post processing and quality control

As shown in Fig. 5, the production process is performed using L-PBF system (i.e., AM machine) made by several sub-systems, which are introduced in the following.

The primary process subsystems include the optical chain, identified by the elements ①-⑦, and the powder feeding system, represented by elements ⑧–⑭. In Fig. 5, the (blue) arrows indicate the degrees of freedom of the moving parts. The production process begins by loading the powder into the supply chambers ⑭. The powder feed pistons and baseplates ⑪ are initially positioned at the minimum excursion (i.e., lowest position), while the building piston and baseplate ⑩ are set at their maximum excursion (i.e., highest position). Layer by layer, alternating left to right supply chambers ⑭, the recoating mechanism ⑨ spreads the powder feed supply ⑫ on the top of the powder bed ⑧, which has been lowered by the height of one layer moving ⑩ down. A fresh layer of powder coated on top of the previous layer is therefore scanned and locally fused by the energy input of a laser beam ⑦. The

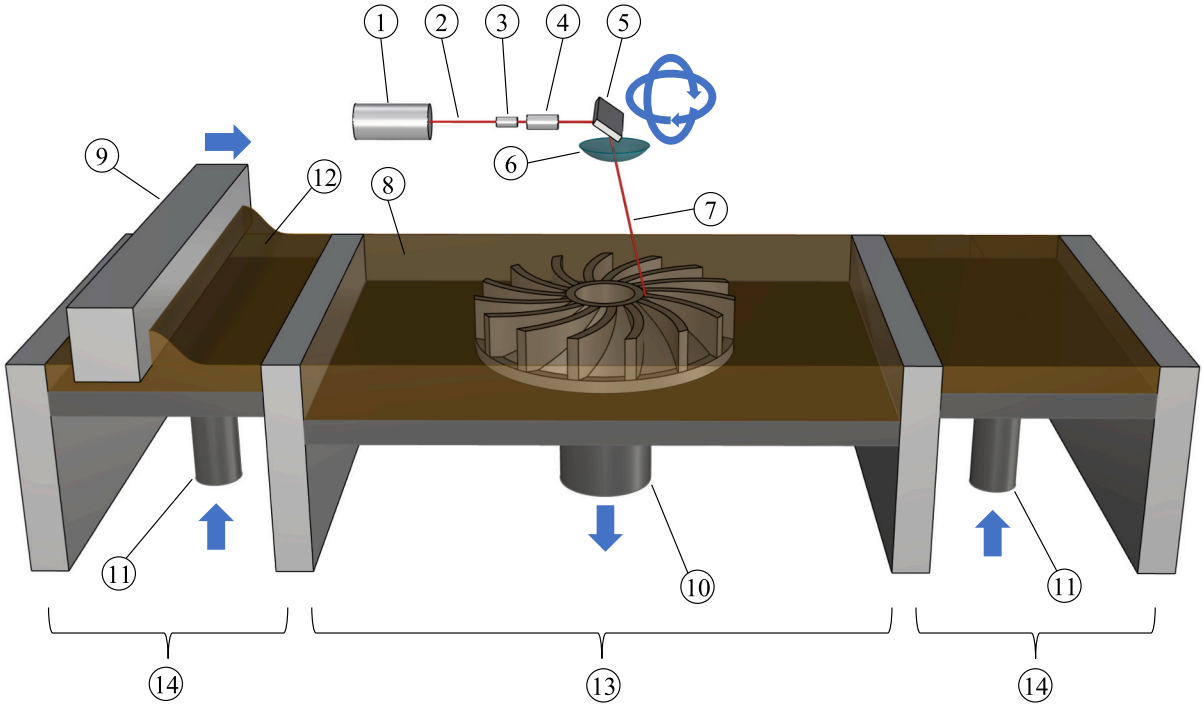

Fig. 5. The L-PBF system and its main components. ①—laser source, ②—laser beam transfer, ③—collimator, ④—beam expander, ⑤—scanning mirror, ⑥— f-theta lens, ⑦—laser beam, ⑧—powder bed, ⑨—recoating mechanism, ⑩—build piston and baseplate, ⑪—powder feed piston and baseplate, ⑫—powder feed supply, ⑬—building chamber, ⑭—powder supply chamber.

laser beam is provided by a laser source ①, transferred by the laser beam transfer ② to the optical components such as collimator ③ and beam expander ④, and deflected by a scanner system. The scanner system utilizes x-y moving mirrors ⑤ driven by galvanometers to accurately position the laser spot along the scanning path. To ensure high precision, the scanner is liquid-cooled due to its sensitivity to thermal deformation. Finally, f-theta lens ⑥ are used to focus the laser beam. This sequence is repeated until the 3D object is completed inside the building chamber ⑬. Typically, the baseplate and powder bed are preheated, and the building chamber ⑬ is protected with inert gas. Excess material can be disposed of in an overflow tank and reused in the next building job [45].

After the actual production process has been completed, several downstream steps are required to finish the AM process. As illustrated in Fig. 4, for instance, the part must be post processed (e.g., removal from the baseplate and cleaning of powder residues). Depending on the application of the manufactured part and the specific requirements, additional post processing steps such as machining, surface, heat, or chemical treatment may also be necessary [45]. Finally, offline quality control is carried out to assess the conformity of internal and external features of the produced part [46,47].

3. Material and method

This research was conducted through a systematic literature review, re-adapting the methodology proposed by [20] and widely used by other academics [48]. In the current article, we introduced a novel deductive approach derived from the Deming cycle [19], which inspired us to explore and categorize the four main drivers considered for online control of metal AM. Table 2 details the steps followed for this review and answers to RQ1: *what aspects do we aim to examine in the literature?*

Using the proposed research string, we performed a query on Scopus [49], the largest database of peer-reviewed scientific literature [50]. A query is a structured sequence of words in the field of Information Retrieval (IR) used to formalize the search of information (e.g., scientific papers, patents, websites) on a given database. Selected keywords are connected by logical elements, such as “OR”, “AND”, “NOT” [51]. After Phase 1–3 we initiated the defined query on Scopus advanced search portal, yielding 217 contributions. Subsequently, Phase 4 involved refining these contributions through automatic inclusion/exclusion criteria, resulting in a reduction to 133 papers. Initially, conference papers were excluded due to their typically lower scientific impact and robustness. In Phase 5, a thorough examination of titles, abstracts, and keywords led to a further reduction to 86 contributions. In Phase 6, we conducted manual refinement via Google Scholar to triangulate the results, incorporating two relevant additional review papers. Recognizing the advantages and limitations of conference papers, i.e., faster publication versus reduced robustness, a threshold of 30 citations was established for inclusion. As a result, 7 conference papers were added. The final set of 95 papers underwent an in-depth analysis to extract information pertaining to each of the four drivers (i.e., input parameters, output signatures, sensing techniques, feedback strategies) as per RQ2: *what are the primary approaches found in the literature?*.

4. The four drivers

In this section, we classified the collected 95 papers into the four identified drivers according to Fig. 2. Table 3 provides details about the classified papers and the corresponding article sections that offer an in-deep review of each driver.

4.1. Input parameters and output signatures overview

In the metal L-PBF process, many different parameters (i.e., over 50) impact the ultimate quality of the finished 3D part [22]. Such complexity creates a significant challenge in understanding process physics and developing an effective process control strategy. According to [17], L-PBF process variables can be identified as process parameters and process signatures.

Table 2
Review protocol according to [20]. Used databases: Scopus [49] (and Google Scholar for triangulation).

Review phase	Detail	Outcome
1. Keywords identification	The keywords identification was driven by the research purpose and the scope of the review. Five main orthogonal concepts (i.e., *location*, *timing*, *goal*, *process*, and *material*) have been defined and instantiated in the specific case by words and synonyms.	*Location*:(in-situ; in situ; inline; in-line; in line) *Timing*:(online; on-line; on line; real-time; real time) *Goal*:(monitoring; control; feedback) *Process*:(selective laser melting; selective laser sintering; powder bed fusion; SLM; PBF; SLS) *Material*: metal
2. Query string development	The operator "AND" was necessary for isolating the previously defined orthogonal concepts that must be (all) embedded in the query outcome. The "OR" operator was used to concatenate semantically similar keywords for a specific concept (synonyms). Please note that despite *location* and *time* concepts are orthogonal, for a broader query we merged these two categories via "OR" operator.	(("in-situ" OR "in situ" OR "inline" OR "in-line" OR "in line") OR ("online" OR "on-line" OR "on line" OR "real-time" OR "real time")) AND ("monitoring" OR "control" OR "feedback") AND ("selective laser melting" OR "selective laser sintering" OR "powder bed fusion" OR "SLM" OR "PBF" OR "SLS")AND("metal")
3. Potential addition of keywords	An initial advanced search was carried out using the Scopus database "Title, abstract, keywords" criteria. The keywords within the papers resulting from this search were then analyzed through Scopus analytics. Current keywords were found to be suitably comprehensive.	TITLE-ABS-KEY(("in-situ" OR "in situ" OR "inline" OR "in-line" OR "in line" OR "online" OR "on-line" OR "on line" OR "real-time" OR "real time") AND ("monitoring" OR "control" OR "feedback") AND ("selective laser melting" OR "selective laser sintering" OR "powder bed fusion" OR "SLM" OR "PBF" OR "SLS") AND ("metal"))
4. Automatic refinement of the identified papers	The papers from Phase 3 were filtered according to the inclusion/exclusion criteria. In particular, the following inclusion conditions were applied: Source type = Journal OR Review OR Conference review OR Book chapter; Language = English; Time window = 2007 – Today (July 2022).	Input: 217 papers Output: 133 papers
5. Manual refinement (exclusion)	During this phase, the titles, abstracts and keywords of the 133 papers were carefully examined to determine their relevance to our research topic and objectives. In cases of uncertainty regarding the exclusion, the entire content was inspected before making the decision to remove the paper.	Input: 133 papers Output: 86 papers
6. Manual refinement (inclusion)	In this phase, the same query was executed in Google Scholar to supplement the results through triangulation. A total of 2 additional review papers were chosen and included into the final set. Furthermore, conference papers that have been previously removed in Phase 4 were reconsidered for further analysis. Abstracts of conference papers with at least 30 Scopus citations were reviewed, leading to the selection of 7 new conference papers.	Input: 86 papers Output: 95 papers
7. Papers review and classification based on the four drivers	The selected 95 papers were reviewed and classified to ascertain their individual contributions to each of the four drivers: input, output, sensors, feedback strategy.	Analysis of the papers

Process parameters are input to the process. They are either potentially *controllable* (e.g., laser power and spot size, scanning speed, layer thickness, scanning strategy) or *predefined* (e.g., laser wavelength, powder bed material and type, inert gas type). The focus of this article will concern controllable parameters used to control the heating, melting, and solidification process, thus maintaining part quality during the process [17].

Process signatures occur during the actual built and are often called "the voice of the process". They are dynamic characteristics of the powder heating, melting, and solidification processes. These signatures are categorized into two classes: *observable* signatures and *derived* signatures [17]. The former can be observed and measured during the process by using in-situ sensing devices and are considered in this article.

Controllable and predefined input parameters are related to the observable and derived output signatures [17]. Thus, developing correlations between input parameters and output signatures support actual closed-loop control, with the goal of embedding process knowledge into future control approaches [4,17,21–23]. This aspect is introduced in Fig. 4 and detailed in Fig. 6, which recall the initial Fig. 2 by offering an overview of the two drivers.

As depicted in Fig. 6, the process's online controllable input parameters (detailed in Sections 4.1.1) and online observable output signatures (described in Sections 4.1.2) were both arranged in three main subcategories (i.e., laser, powder bed, and building ambient). For those readers interested in a broader overview on predefined parameters (in addition to the ones highlighted in Section 2) and related signatures, which are not in the scope of this article, the following extensive reviews are suggested [17,22].

In the following Table 4, the retrieved papers are classified based on the highlighted categories in Fig. 6, following the preliminary classification adopted in Table 3 for these two drivers.

4.1.1. Online controllable input parameters

4.1.1.1. Laser. As for online controllable laser parameters, the laser power (P) and the scanning speed (v) identified in Fig. 6 are crucial to define the amount of energy transferred in the affected zone [22]. While the power indicates the amount of energy transferred per second, the speed determines the time spent in the same area. Therefore, equilibrium between these two parameters avoids the formation of defects (e.g., pores) [52]. The scanning strategy is another parameter suited for online control and deals with the pattern that the laser beam follows to irradiate the selected region of the powder bed. Given a specific scanning strategy (e.g., the zig-zag strategy shown in Fig. 6), the laser beam moving along that path at a certain scanning speed over the powder [53]. Moreover, during the L-PBF process, it is possible to shift the laser beam focus or defocus by displacing the building piston and baseplate ⑩ in Fig. 5 along the z axis to increase laser spot size (d). The diameter of the spot can influence the energy transmitted and the area affected by the powder bed [54].

4.1.1.2. Powder bed. When focusing on the powder bed, the recoating speed (r), dosing (d) and compression (c) of the powder are others online controllable input parameters that have direct influence on the final density and quality of the printed parts [55]. Another parameter to consider is the layer thickness (t), which refers to the spacing between layers [56]. Notably, thicker layers can result in larger sizes, potentially elevating the melt pool temperature [56]. The hatch space (h) parameter refers to the distance between centers of adjacent laser beam tracks [57].

Table 3
The 95 pertinent papers collected and classified according to the four drivers and their respective article sections.

Article section	Description	Relevant review papers	Other papers (review/research)
4.1.1 Online controllable input parameters	Key input parameters that can be controlled during the metal L-PBF production process	[4,17,22,23]	[52–59]
4.1.2 Online observable output signatures	Primary online observable output generated by a metal L-PBF production process (i.e., signatures)	[4,17,22,23]	[18,55,59–82]
4.2.1 Online sensing techniques	Primary sensing techniques employed for online monitoring of metal L-PBF production processes	[4,18,21–23,83,84]	[52,54,63,65,69,78,79,84–138]
4.2.2 Online feedback strategies	Primary feedback strategies for implementing online corrective actions in the metal L-PBF production process	[17,22,23,42]	[139–141]

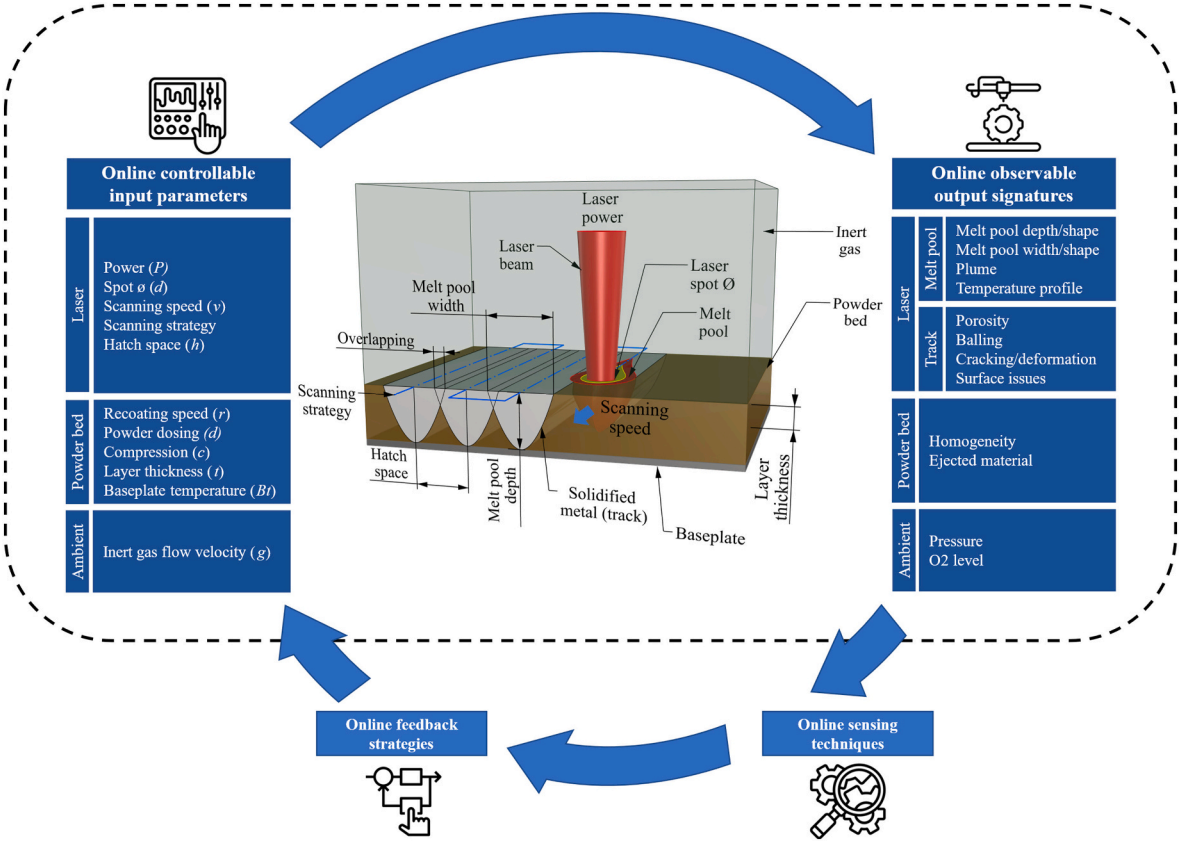

Fig. 6. Expanded version of Fig. 2. Classification of the online controllable input parameters in the L-PBF process (left). Classification of the online observable output signatures in the L-PBF process (right). Schematic representation of L-PBF along with labels for some controllable input parameters and observable output signatures (center). The light blue arrow in the schematic representation highlights the direction of the laser beam, and the light blue dotted path illustrates the scanning strategy.

Table 4
Manual labeling of the pertinent retrieved papers concerning the online controllable input parameters and output signatures.

Driver	Laser	Powder bed	Ambient
Online controllable input parameters	[22,52–54]	[55–58]	[59]
Online observable output signatures	**Melt pool**: [60–69] **Track**: [18,70–78,81,82]	[55,79,80]	[22,59]

Lastly, the base plate temperature (*Bt*) stands as another online controllable parameter with a notable impact on the powder bed temperature. This temperature regulation proves significant in reducing thermal stresses in SLS/M parts, achieved through the mitigation of process thermal gradients [58].

4.1.1.3. Ambient. As for the ambient (or built environment) and other unwanted reactions, inert gas is fed through the build chamber to create an inert atmosphere to avoid oxidation. In this case, the direct online controllable parameter is the gas flow velocity (*g*). This influences directly other characteristic of the chamber (e.g., relative pressure and oxygen content) and indirectly the quality of the manufactured part [59]. In addition to the shielding properties of the inert atmosphere, the gas flow velocity is directly responsible for the removal of spatter and welding fumes originating from the process zone [59].

To conclude the overview about online controllable input

parameters, it is necessary to introduce a Key Performance Indicator (KPI) defined by aggregating some of the process parameters described above and used to characterize the process. The laser power (P) measured in (W = J/s) divided by the scanning speed (v) measured in (mm/s), together with the hatch space (h) measured in (mm) and the layer thickness (t) measured in (mm), define one of the most critical KPI, namely the energy density $E_d = P/htv$ (J/mm^3) [59].

4.1.2. Online observable output signatures

4.1.2.1. Laser (melt pool). Melt pool (c.f. Fig. 6) is the primary class of online observable signatures that involves any process dealing with a laser beam aimed at achieving a local fusion of the material [60]. In the literature, numerous melt pool related signatures have been considered for monitoring purposes [61,62]. Geometrical features such as width, depth and relative cross-sectional shape of the molten material have been treated to some extent to monitor the process stability [63]. Under laser processing, the temperature gradient determines the speed of phase transitions, chemical reactions, microstructure, and material properties [64]. Melt pool temperature (1D, 2D, and 3D profile [65,66]) is, therefore, one of the most dynamically studied signatures [67,68]. The plume is another signature which can be observed during the laser processing. It is formed by the partial material vaporization, which may also lead to the formation of plasma because of metallic vapor ionization. The plume differs from the surrounding atmosphere, and it can interfere with the optical properties of the laser (e.g., beam profile and local energy density) [69].

4.1.2.2. Laser (track). Track (or solidified material) is the second class of online signatures related to the material affected by the laser beam. As shown in the graphical representation of Fig. 6, once the melt pool solidifies, the material turns into a solid track [71], which significantly impacts the final quality of the part due to defects [70]. Among main observable online defects deriving from the melt pool solidification, porosity, balling, surface issues and other (e.g., cracking and deformation) should be considered [4,72]. Porosity consists of voids inside the bulk of the fused material [73]. Two separate mechanisms mainly determine the formation of such pores. The first is an incomplete melting of the powder because of low power or high scan speed [81]. The second is the "keyhole effect" (i.e., melt pool's material is vaporized, resulting in a bubble-like cavity upon solidification), often caused by high power or low scan speeds [74]. The formation of solidified balls of material on the part surfaces after melting (i.e., balling) often occurs where the powder used in an L-PBF process has high surface tension in the liquid phase [4]. These balls can form highly rough surfaces or pores between two or more balls when in contact, and similarly to the previously presented defects their monitoring is crucial [75]. Residual stress is another significant issue in AM-manufactured metal parts, and often the thermal gradient mechanism and the cool-down phase of molten top layers cause cracking (e.g., delamination) or geometric deformation [76,77,82]. Others geometric and dimensional issues (e.g., stair-case effect, shrinkage, and displacement) can occur during the processing [18] as well as surface defects and roughness which are a significant factor in the fatigue and crack nucleation [78].

4.1.2.3. Powder bed. As shown on the right side of Fig. 6, another class of observable output signatures encompasses those associated with the powder bed. Signal acquisition in this context can be executed subsequent to (or during) the deposition of the powder bed itself, prior to the laser sintering or melting of the following layer. Within this realm of signatures, ensuring the homogeneity of the coated powder stands out as a particularly critical aspect for monitoring. Some papers demonstrate that during the recoating process, numerous defects might arise, and ununiform distribution of the powder can be detected [55]. Moreover, powder bed monitoring of fused clumps of powder or ejected material (i.e., spatter) from the melt pool has been reported [79]. Spatter can be classified as droplet spatter and powder spatter, both arising because of the impact of metallic vapor [80].

4.1.2.4. Ambient. The final set of observable signatures which influence the process stability and, therefore, the part quality concern the inert gas of the building chamber [59]. Oxygen (O_2) level is probably the most critical process environmental signature on the quality metrics [59] since oxygen can lead to oxide formation in metal, change wettability, and energy required for welding. Ambient relative pressure and temperature are also important signatures to be controlled during the production process. The former influences vaporization of metal as well as oxygen content. The latter impacts heat transfer, powder preheat, and residual stress [22].

4.2. Sensing techniques and feedback strategies overview

As detailed in Section 2, the laser beam scans at a controlled scanning speed the selected locations of the powder bed. Then, it fuses the powder to the solid material underneath by either complete melting (i.e., SLM) or partial melting (i.e., SLS). A single layer of metal is "cast" upon a previous layer resulting in complex correlations between online controllable input process parameters and online observable output process signatures. The result is that there is a need for real time, closed loop process feedback and sensors to ensure quality, consistency, and reproducibility by online adjustment of the input parameters based on observed signatures [17].

Although numerous papers provide an overview on the application of sensing techniques (i.e., 3rd driver) for monitoring purposes in metal L-PBF [4,21–23,83,84], a structured classification of the sensors and their application on L-PBF following the approach presented in Fig. 2, is missing. Moreover, as for feedback online strategies (i.e., 4th driver), only a few studies have been published regarding an actual implementation of either reactive, corrective, or feedback control actions for metal SLS/M process based on detected signatures. For this reason, the pre-classified papers of Table 3 are analyzed also in this context.

According to the article outline, Fig. 7 recalls the initial Fig. 2 by offering an overview of the two drivers treated in this section. In Section 4.2.1, a classification of sensors suitable for online, in-situ, metal SLS/M signature monitoring based on two types of physical responses (i.e., electromagnetic, and acoustic) retrieved by the literature search are proposed, and subclasses are generated on reviewed papers (Table 5). As shown by Fig. 7 these sensors, after data processing and analysis provide the information necessary for the online feedback strategies reviewed in Section 4.2.2.

4.2.1. Online sensing techniques

As shown in Table 5 and accordingly to our query output, the electromagnetic signals class covers a series of sensors that work in a broad range that copes X-Ray (XR), visible light till the Near InfraRed (NIR) and IR wavelengths (from 0.01 to 2300 nm). In this class also multispectral emission spectroscopy (i.e., within specific wavelength ranges across the electromagnetic spectrum) have been labeled. Regarding general information, irrespective of the sensor type, the mounting method involves two main approaches: co axial and off axial systems. In co axial configurations, the sensors utilize the optical path of the power source. In off axial configurations, the sensors are positioned outside the optical path, with a specific angle of view for the region of interest [4]. Acoustic sensing is the second category that the authors identified in the retrieved papers. In this case, no specific subclasses have been labeled.

Standard sensors (e.g., velocity and spatial transducer) nowadays widely embedded in Numerically Controlled (NC) machines aiming for controlling specific input parameters are out of the scope of the following classification. Commercial sensing solutions for online signature monitoring are out of scope as well. The following accurate papers

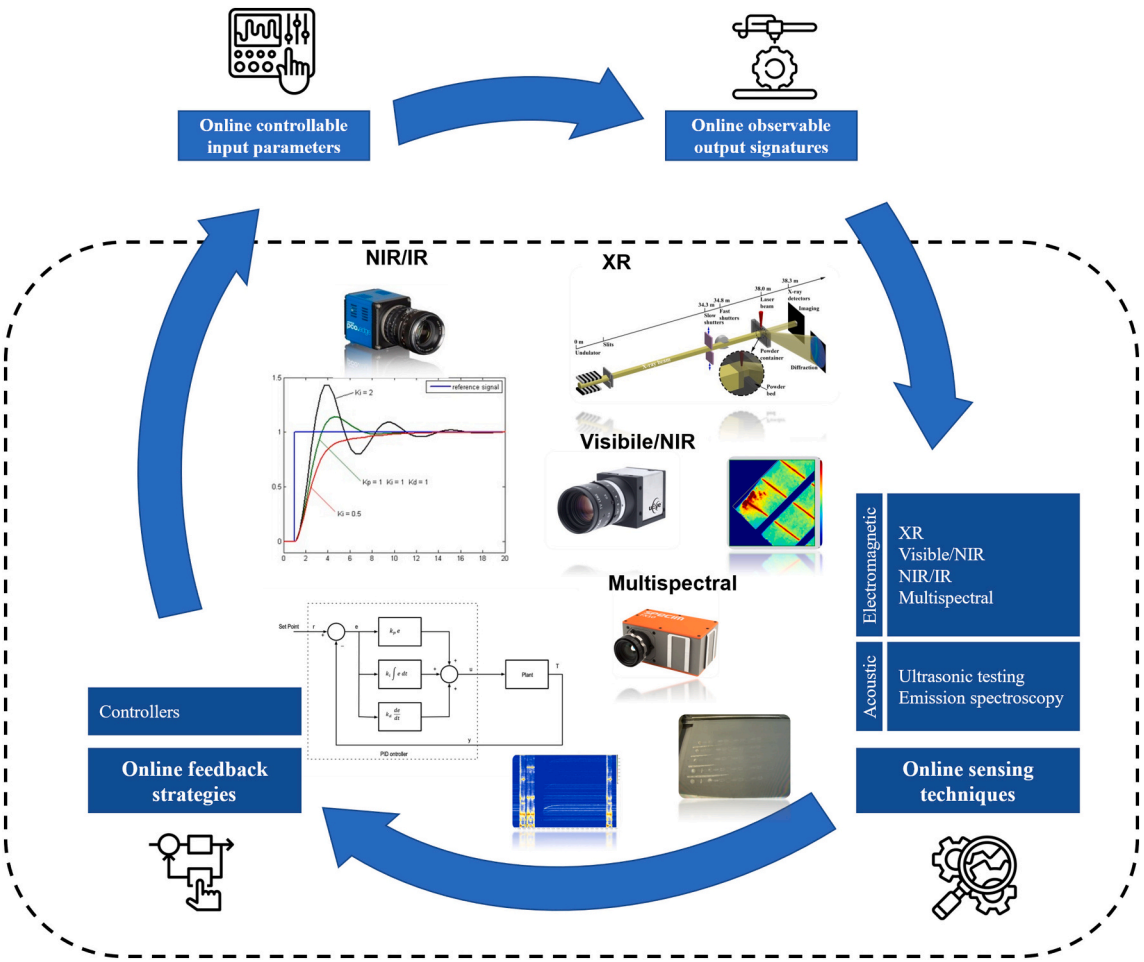

Fig. 7. Expanded version of Fig. 2. Classification of common in-situ sensors suitable for monitoring online observable output signatures and depiction of online feedback strategies applied in literature.

Table 5
Manual labeling of pertinent retrieved papers for the electromagnetic and acoustic source sensing approach. All sensor types have been organized to emphasize and summarize crucial features (such as sampling rate, cost and time, #retrieved papers, signatures detectable and references to retrieved papers).

	Sensor type	Sampling rate [kHz]	Costs and time consuming	Number of papers retrieved	Signatures detectable	Retrieved papers
Electromagnetic	*XR*	50	High	5	*Melt pool*: depth/shape *Track*: porosity, balling, surface issue *Powder bed*: ejected material	[52,63,85–87]
	Visible-NIR	>1–900	Low	26	*Melt pool*: width/shape *Track*: porosity, balling, crack/deform, surface issue *Powder bed*: ejected material, homogeneity	[54,79,88–110,136]
	NIR-IR	0.05–10	Low	19	*Melt pool*: width/shape, plume, temperature profile *Track*: porosity	[65,69,84,111–124,133,134,138]
	Multispectral	0.01–170	Medium-high	3	*Melt pool*: width/shape, plume, temperature *Track*: porosity, surface issue	[125–127]
Acoustic	*Sonic or ultrasonic*	3 - >20	Low	8	*Melt pool*: depth and width *Track*: porosity, surface issue *Powder bed*: ejected material	[78,128–132,135,137]

can be considered for more details [4,18,21].

In Fig. 8, we present a visual summary of the comprehensive review of sensing techniques for monitoring purposes analyzed in the following sections. The left side (Fig. 8a) displays two bar graphs, illustrating the citation count and maximum cited paper at the top, and the publication count and H-index according to the Scopus database at the bottom. These metrics are reported for each reviewed sensing technique, providing insights into the quantity and quality of published papers categorized by sensor types, and reinforcing the information initially provided in Table 5. Notably, Visible-NIR and NIR-IR sensors

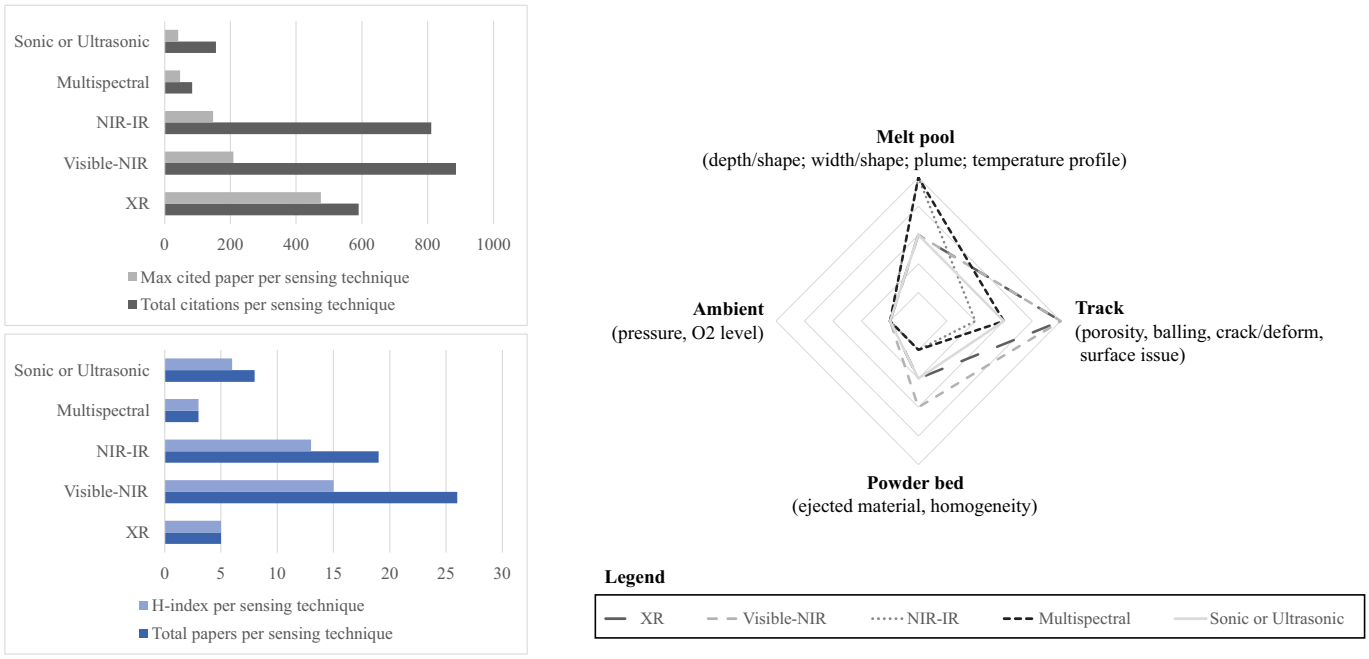

Fig. 8. (a) Last decade of published papers on online sensing techniques and (b) extent of coverage of monitored signatures using each specific sensing technique.

demonstrate extensive academic resonance, being the most cited and presenting the highest H-index. Lower scientific relevance is associated with multispectral approaches, while XR and sonic or ultrasonic (i.e., acoustic) sensing techniques gather certain interest but are still far from visible-NIR and NIR-IR.

On the right side (Fig. 8b), a radar graph visually represents the number of covered signatures by each specific sensing technique, based on the information summarized in Table 5. Again, Visible-NIR and NIR-IR sensors demonstrate extensive coverage, encompassing a wide range of signatures (i.e., NIR-IR for melt pool and visible-NIR for track and powder bed). Regarding ambient signatures, no scientific papers have been retrieved addressing this aspect from a sensing perspective.

Based on the above observations, it is evident that Visible-NIR is frequently employed in conjunction with NIR-IR systems (laser wavelength and pool thermal signature), as discussed in Section 5 (see Section 6, data variety).

In the following Sections 4.2.1.1-4.2.1.5 we provide a detailed review of the retrieved papers for sensing techniques dived in the identified classes and subclasses (Table 5).

4.2.1.1. XR. Ultra-fast in-situ real-time XR imaging seems to be the one of the most promising technique due to its relatively recent introduction and continuous growth during the years. At the same time, compared to other techniques suffer for less flexibility and more costly and time expensive set-up. As introduced by one of the first studies in [85], scientifically and technologically significant phenomena in metal L-PBF (e.g., melt pool dynamics, keyhole porosity, powder ejection and phase transformation) can be monitored via XR. On this initial stage, additional papers have been published and an open architecture prototype of a compact XR system was reported in [86]. A step further in high-speed synchrotron XR imaging has been introduced by [63]. Similarly, to the previous papers, they used a horizontal set-up (the laser had an angle of incidence of 7° relative to the sample surface normal) and 50 kHz frame rate. As main result, the authors correlate the projective melt pool geometries to laser absorption proposing the use of a total backscattered light detection system for real time process control of keyholes, melt pool's aspect ratio deviations, and instabilities [63]. Furthermore, in [52] the authors propose an experiment on pulsed wave metal L-PBF to study the cavity and porosity pattern formation (i.e., melt pool dynamic), which is a well-known issue in this operating mode [52]. Similar to [63] but more recent study has been reported by [87]. By simultaneous in-situ synchrotron XR (50 kHz frame rate), the authors directly probe the interconnected fluid dynamics of the vapor jet formed by the laser and the depression it produces in the melt pool demonstrating how unstable keyhole is accompanied by a transition to chaotic flow in the plume [87]. In the present article, the contribution on XR Computed Tomography (XCT) has not been included due to the conventional off-line (i.e., post-process) inspection. This technique is only mentioned as a comparison (i.e., ground truth) to online techniques.

4.2.1.2. Visible-NIR. Meanly dealing with visible or NIR spectra, digital imaging is often associated with vision systems, which nowadays are tremendously adopted both in the industrial and consumer industry using spatially resolved sensors such as Charge Coupled Devices (CCD) and Complementary Metal Oxide Semiconductor (CMOS) [88]. Due to the flexibility, low cost, and continuous improvement of visible/NIR imaging techniques, they have been adopted for decades in laser-based manufacturing and its level of adoption is at an early maturity stage. Among the reviewed articles, in [89] a high-speed camera (10 kHz) was utilized with telescopic lenses to monitor the interaction of laser parameters (i.e., power and speed) and material signatures (i.e., melt pool and spatter). In another paper, the authors present a system based on a camera with 300 kHz frame rate as a compromise between the capability of capturing the laser kinematics and the computational feasibility of in-process image analysis [90]. A similar approach was applied also in [91,92] on high frame rate cameras (1–25 kHz) some years later. In the same year of [90], another step forward in the processing of image datasets generated from optical camera has been introduced by [93]. In their paper, the authors used a fixed (off-axis) field of view camera ranging in the 6–900 kHz frame rate and propose a method to transform the high-speed image data such that the melt pools appear as viewed through a coaxially aligned optical setup. In 2019 a supervised learning technique (i.e., Bayesian inference) was proposed as a solution for quasi-real-time (layer-wise) track (e.g., pores/surface issues) control [94]. Real time monitoring systems to enhance repeatability and quality control using collected videos to train CNNs with a semi-supervised

model are proposed by Yuan et al. [136]. These papers opened the era of ML adoption in the optical imaging monitoring (and even forecasting) as demonstrated by the significant amount of optical sensing and ML contributions in the recent years [95–105]. Papers specifically focused on spatter analysis were published in [79,106,107]. Other relevant papers, such as the one published in 2019 by [108], report high-resolution in-situ monitoring for the identification of optical features correlated with the part density and mechanical properties. Similar papers based on layer-wise optical control of defects on the layer surface were proposed in [54,109]. On the other hand, in [110] the author proposed an optical dimensional measuring method coding the surface profile layer with structured light, which is recorded by a CCD camera. The point cloud coordinates output are compared with the CAD model to detect errors in powder coating or layer thickness consolidation. Finally, we report another paper that proposes an online optical system based on industrial cameras to collect images and detect SLM powder bed spreading issues (e.g., powder bed surface homogeneity) [97]; for this specific application a low frame rate has been demonstrated to be sufficient (0.023 kHz).

4.2.1.3. NIR-IR. Heat transfer is a driving force of the L-PBF [111]. The formation and dynamic behavior of the molten pool as well as the liquid metal cooling and solidification have a direct impact on microstructure, residual stress, and deformation of components. Spatially integrated single channel sensors (e.g., photodiodes and pyrometers) have widespread use in melt pool monitoring of advanced laser processing as well as cameras with special wavelength filters and frame rates [84]. A layer wise approach based on relative surface temperature (i.e., thermal radiation) measurements was developed for subsurface defects identification (e.g., lack of fusion) [112]. Another layer wise approach was proposed by [113]. In this paper, the authors used a high-speed (100–250 Hz) thermal imaging system (i.e., dual-wavelength imaging pyrometer with temperature range 1500–2500 °C) to capture melt pool temperature variations. Similarly, in [114] two-color pyrometry data sets were used to estimate instantaneous temperatures, melt pool orientations and aspect ratios [114]. Further application of pyrometers adoption for melt pool temperature analysis can be retrieved. For example, [115] proposed melt pool temperature time series analysis via ML for pores detection using a 100 kHz pyrometer as sensing source. Additionally, temperature distribution in the sintering zone has been studied using a video camera, along with maximum surface temperature control in the irradiation spot using a high-speed two-wavelengths pyrometer [133]. Other examples using IR camera and pyrometer applied for SLM process visualization and control can also be found varying the sampling rate from 2 to 3 kHz [134]. In a more recent paper, another application of ML is proposed for IR data obtained from a thermal camera (50 Hz) [116]. Other applications on online monitoring of melt pool geometry (i.e., width/shape) were carried out via IR camera with 58 Hz frame rate and a working range 600–3000 °C by [117]. Similarly, a methodology for IR imaging feature extraction was proposed by [65,138]. In [118] the authors proposed an approach based on IR images acquired with an off-axial IR camera (50 Hz frame rate) to detect possible deviations of plume from a stable behavior in AM zinc powder processing (temperature range 100–500 °C) [118]. Additional papers on processing thermal videos captured during the SLM of zinc powder are reported by the same research group [69,119]. Furthermore, a Short-Wave Infrared (SWIR) thermal camera (2.5 kHz frame rate) measurements to compile voxel-based part representations and understand how the complexities in the thermal history affect part performance was proposed by [120]. The same author proposes an updated version of the previous paper using SWIR thermal camera for porosity probability mapping [121]. Among the most recent papers, [122] details a design and validation for an online in-situ monitoring system for the detection of some melt pool signatures (e.g., temperature profile, temperature gradient, cooling rate) [122]. Recently, another in-process thermography as an in-situ monitoring tool was presented by [123]. To conclude we also report a novel alternative set-up for investigating the melt pool in the cross section, based on high-speed (10 kHz frame rate) thermographic camera mounted orthogonally to the scanned plane behind a glass [124].

4.2.1.4. Multispectral. As opposed to the previously reviewed techniques, multispectral emission spectrometry counts a few published papers. Despite Optical Emission Spectroscopy (OES) has previously been implemented in laser welding processes for plume (e.g., chemical species and temperature) and melt pool features (e.g., depth to width) as well as DED process monitoring, it seems that these approaches for metal L-PBF are novel and at an early adoption stage [125,126]. In more details, in [125] the spectrometer is split into the laser beam path of the SLM system to measure the visible light emitted from the melt pool size and plume in-process at 14 Hz frame rate and correlated it with the melt pool properties of samples. OES has been proved to be useful also for SLM porosity monitoring. As described by another paper, optical emission signatures can be captured via in-situ multispectral photodetector sensor at 100 kHz frame rate [126]. Accordingly to the authors, the porosity-level within each layer of a test part was quantified using XR Computed Tomography (CT) as ground truth to train a ML model that take OES data as input and predict the percentage porosity-level in each layer. This approach is found to predict the porosity on a layer-by-layer basis with an accuracy of ~90 % in a computation time <0.5 s [126]. A more recent paper still based on ML prediction model proposes a dataset obtained via an area-scan hyper fast (170 kHz frame rate) hyperspectral (i.e., from across the electromagnetic spectrum) camera as input to predict the surface roughness [127]. The hyperspectral images obtained from the process were labeled with the surface roughness as determined by a confocal microscope and used to train a Convolutional Neural Network (CNN). Overall, the results suggest that hyperspectral data does provide crucial information about the L-PBF process, and that hyperspectral imaging could potentially help establish on-line product qualification [127].

4.2.1.5. Acoustic. Electromagnetic monitoring methods reviewed in the previous sections are common but are mainly limited to observing only the surface of the AM build (except XR). Acoustic sensing either inducing sonic or ultrasonic waves, is broadly adopted for nondestructive testing, and monitoring internal features (e.g., porosity) [128] due to the simplicity and low cost of the related sensors (i.e., microphones) [4]. Acoustic Emission (AE) techniques are based on sonic or ultrasonic sensors, which receive waves that relay back information about the inside and have been proposed for in-situ process monitoring [135,137]. A first class of retrieved papers rely on Laser Ultrasonics (LU), which uses lasers to generate and detect ultrasonic waves and produce images known as B-scans and C-scans. For example, the authors of [128] propose an LU technique for porosity measurements. In their paper, the authors explore the current capability of the LU testing technique to detect subsurface defects in metal L-PBF in comparison to XR CT [128]. Another paper based on LU testing in presented in [78]. Here the authors established a system to detect the surface defects of SLM samples that have a different surface roughness. The influences of the surface roughness on the LU signal-to-noise ratio distribution and defect sizing accuracy were studied as well [78]. Other papers focused on the air-born acoustic emission generated due to the SLM laser interaction to the material [129]. In their paper, the authors report the utilization of a microphone mounted in the building chamber sampling acoustic data at 100 kHz for porosity formation (i.e., keyhole mode) monitoring. Similarly, [130] proposed a method based on the in-process acoustic signals monitoring via a microphone. Finally, we recall the recent paper from [131] in which an ultrasonic time of flight measurement monitoring technique is numerically and experimentally used to study the behavior of laser-induced melting pools, including depth and width estimation as

Table 6
Pertinent retrieved papers concerning control strategy and their features comparison.

Paper	Control strategy	Paper Contribution to control	Practical application	Computational requirements
[139]	PID control embedded in Additive Manufacturing Metrology Testbed NIST	Practical implementation and experiment of a control system and proposal of Geometric Conductance Factor (GCF) calculation: Melt pool solid/liquid factor	Yes	Low
[140]	Intelligent compensation architecture based on online and offline control loops	Theoretical presentation of control loops (Airflow circulation, Powder filling and spreading, Laser galvanometer)	No	Moderate
[141]	Model Predictive Control (MPC)	Comparison of online PID controllers in contrast to offline ML-based predictive model	No	High

well as phase transition and other dynamics in real time [131]. To conclude, the most recent retrieved paper is about the application of transfer learning (i.e., a paradigm where a model already trained on a similar task is re-used with minimum training to accomplish a new task) to improve current ML generalization for online monitoring of different metals in SLM [132]. In their paper, the authors propose the utilization of AE spectrogram on a certain metal for capturing acoustic data correlated to specific signatures (e.g., pores, balling) and retrain the already trained model to other metals via material-specific spectrograms [132].

4.2.2. *Online feedback strategies*

As highlighted by several authors, because of the L-PBF process complexity (i.e., over fifty input parameters and as many observable signatures), actual feedback on AM machines is still far from the industrial application [17,22]. To date, the L-PBF process is an open-loop control system with several in-situ monitoring capabilities (Section 4.2.1). Unfortunately (and typically), a trial-and-error approach is adopted to set up experimental parameters, which are fixed throughout the entire build process. These approaches are insufficient to ensure part quality since parameters need to be dynamically adjusted in response to the underlying evolution of process signatures [23,42]. Despite the lack of standard control protocols for L-PBF AM systems, in this section we report the restricted set of retrieved articles that propose an actual feedback control system and closed-loop strategy in detail.

As reported in Section 2, most AM processes start from a CAD file and the creation of digital position commands for galvo and power laser control as a series of x-y-power entries stored into the G-Code. One the most used protocols for galvo control is the xy2–100 [139]. In this protocol, the digital position commands are packaged into 20-bit packets and transmitted at 2 MHz clock rate to the galvo digital-to-analog (D/A) receiver, converted to analog voltage to drive the galvo motor through a local Proportional-Integral-Derivative (PID) loop. Similarly, the laser power on most commercial laser units can be controlled through an analog voltage input, where the digital power command can be transmitted and converted (D/A) as galvo control signal [139]. According to the above, the authors of [139] propose a feedback control system for controlling the laser power in an L-PBF process based on locally varying signatures (i.e., relative proportion of solid or powder material near to the melt pool) [139]. A factor called the Geometric Conductance Factor (GCF) was calculated, and laser power was linearly scaled to the GCF throughout the build modifying the power of the x-y-power array in real time for overhangs and edges. The algorithm was implemented on the controller of the National Institute of Standards and Technology (NIST) open Additive Manufacturing Metrology Testbed (AMMT) system, and the in-situ melt pool intensity was measured via high-speed (10 kHz rate frame) camera, configured for co-axial melt pool monitoring [139]. As shown in Table 6 this contribution offers a practical and valuable application to the field of control.

Another interesting application of feedback control can be found in the work of Adnan et al. [140]. In their research, the authors proposed a feedback system based on a novel intelligent compensation architecture consisting of two systems (i.e., System1 and System2). System1 is considered as the primary control function and is designed for real time control of the L-PBF machine's discharging, coating, and polishing loops, utilizing its fast and intuitive capabilities. On the other hand, System2 is developed as a secondary tuning function, employing a Melt Pool Images (MPI)-based approach with a CCD coaxial camera and a hybrid model classifier based on ML tools, such as Convolutional Neural Networks (CNNs) and Long Short-Term Memory (LSTMs). System2 aims to determine and assess the appropriate thresholds and parameters of System1 based on the ratios of different MPI classes in an offline manner [140].

Lastly, another paper on actual online control presented a theoretical approach and a valuable comparison between PID control (i.e., the industry standard) and Model Predictive Control (MPC) in maintaining the required melt pool width and depth, controlling laser speed and power [141]. One of the primary advantages of PID is its effectiveness when a qualitative relationship between the desired output and control input is known. After some parameter tuning, control can be conducted without the necessity of a physical model. For the L-PBF process, if melt pool width or depth is below the desired value, increasing the laser power is a well-established solution. Similarly, if laser scanning speed is among the control inputs, reducing the scanning speed is known to increase both melt pool width and depth at the same laser power level. In all cases, PID controllers require direct observation of controlled performance to derive an error term for determining control actions. The capability for in-situ monitoring, as reported in Section 4.2.1, indicates that melt pool features can be observed in real time through various sensing techniques, with some constraints on the sampling rates in the order of kHz. However, when multiple control inputs are used to control the output response, there is a lack of mechanism to coordinate or optimize these inputs for achieving improved control output. Furthermore, when control objectives involve both observable and indirectly observable outputs, along with multiple control inputs, the effectiveness of the PID control comes into question [141]. For these reasons, the authors proposed advanced MPC. While such models are computationally expensive, they are significantly more flexible in producing results under different settings. They can be conducted offline but are closely associated with ML.

Supervised ML involves training a model on labeled datasets, where the relationship between input data and output is known. The model learns from these labeled examples to predict outcomes for unseen data. In the context of L-PBF, supervised learning algorithms can be employed to classify defects, predict temperature distributions, or estimate part quality based on sensor data (i.e., regression). On the other hand, unsupervised ML involves training a model on unlabeled datasets, where the structure and patterns in the data are not explicitly known. By continuously monitoring the process, such models can detect abnormal conditions that might lead to defects or process failures [24,103,142,143]. Semi-supervised ML, as advanced technique, utilizes both labeled and unlabeled data, combining the benefits of both supervised and unsupervised approaches. Another advanced approach is reinforcement learning, which incorporates an intermediary level of information into the algorithm. It is assumed that the training data will provide intermediate level of information about the true and false results. In this case, the system becomes "intelligent" in a trained environment based on rewards or punishments linked to the accuracy of the results. Furthermore, hybridization represents the frontier of research

where multiple models are adopted to optimize the overall system's performance, "leveraging" the strengths of different approaches to achieve enhanced results [24,104,141–143].

According to the above, MPC first requires a physical model to conduct the control (e.g., Finite Element (FE) models that can predict the melt pool size (e.g., length, width, and depth)) under different process parameter settings and assumed boundary conditions. Secondly, supervised ML algorithms are trained based on the generated datasets from FE models. The third step is to further characterize the inherent model bias under different process parameter settings, and to quantify the uncontrollable process uncertainty (e.g., powder and laser property) presented in the experiments. The final updated ML model can be considered as a digital representation (or digital twin) of the physical process [141].

5. Results and discussion

In Section 4, the four proposed drivers for an online control of metal AM have been reviewed. We focused on the logical loop of the Deming cycle (aka PDCA) and considered the 95 papers resulting from a structured literature review method proposed in Section 3.

- Firstly, the online controllable input parameters (i.e., 1st driver) were reviewed in Section 4.1.1 as the planning step (i.e., P)
- Secondly the online observable output signatures (i.e., 2nd driver) were treated in Section 4.1.2 as the result of the doing step (i.e., D)
- Thirdly the online sensing techniques (i.e., 3rd driver) were addressed in Section 4.2.1 as the monitoring or checking step (i.e., C)
- Finally, the few actual online feedback strategies (i.e., 4th driver) retrieved were reported in Section 4.2.2 as the corrective actions or act step (i.e., A).

Online feedback strategies outlined in Section 4.2.2 use in-situ sensors (identified Section 4.2.1) to collect data of online observable output signatures (defined in Section 4.1.2) and adjust in real-time the related online controllable input parameters (defined in Section 4.1.1). From the review of the previous sections, it is possible to derive a few final considerations for each driver and answer to the RQ3: *what are the key findings from the literature?*

5.1. Input parameters/output signatures

The L-PBF process has undergone extensive study and analysis, resulting in the establishment of a universal hardware architecture (AM system or machine) and a specific physical process (selective fusion of powder using a laser beam). Consequently, the input parameters and output signatures of the process are well-defined and categorized. Fig. 6 and Table 4 provide a summary of the first two drivers. However, it is widely acknowledged in the literature that directly applying physics heat transfer or fluid dynamics equations to metal system is unfeasible due to various uncontrolled contingencies that impact each layer's fabrication [144]. For laser-based material processing, DoE based Response Surface Methodology (RSM) is commonly utilized for process development and determining processing parameter values that yield desired properties to avoid anomalies [142]. While there has been significant research on experimentally and analytically understanding the correlations between input parameters and output signatures (e.g., laser power/speed and melt pool signatures), the complexity of the overall phenomena requires more advanced data driven approaches.

5.2. Sensors

Drawing on numerous papers providing an overview of sensing techniques [4,21–23,83,84], this article presents a structured classification of sensors and their application in L-PBF, following the innovative approach presented in Fig. 2 and detailed in Fig. 7. Table 5 summarizes the correlation between sensors and process signatures. The reviewed sensors, extensively discussed in recent literature and undergoing significant development in recent years, enable the monitoring of all significant (i.e., useful) process output signatures. However, despite the progress in sensor development, implementing an efficient and structured sensor architecture in AM industrial applications remains a challenging goal. While many papers focus on specific aspects of sensing, there is still a lack of a general overview and a comprehensive cost-benefit analysis. Based on the reviewed papers of Table 5, it is evident that among various sensing techniques (i.e., XR, visible-NIR, NIR-IR, multispectral, acoustic), significant research attention is directed towards visible-NIR and NIR-IR sensors, as depicted in Fig. 8a. This emphasis can be attributed to their ability to offer cost-effectiveness, simplified installation, and fast calibration processes. However, the primary reason lies in the extensive coverage of process signatures as depicted in Fig. 8b.

5.3. Control

Despite the interesting papers that have been reviewed, the central message conveyed by this article is the noticeable void in the literature concerning the practical application of closed online control loops in metal AM. Out of the 217 reviewed papers, only one presents an actual implementation of online control, and just two others offer comprehensive theoretical approaches that necessitate a digital twin of the process (Table 6). This highlights the need for increased research attention in this crucial realm in the forthcoming years. As depicted in Fig. 4 and serving as a facilitator for the concept of external offline loops, the closed-loop system not only provides real time control but also generates invaluable data that can be stored for continuous process improvement. Through the analysis of historical sensor data and corresponding adjustments in process parameters, manufacturers can gain insights into process trends and performance. This data-driven feedback loop enables refinements in ML models and process strategies, leading to further optimization of the AM process over time.

6. Outlook and open challenges

As discussed in the previous sections, researchers developed advanced sensing techniques for big data collection and maturity on sensors seems to be reached. On the other hand, ML is now the new frontier of research for big data processing, which is strictly related to sensors and control. The big data concept has never been so suited as for this context by defining the 3Vs (Velocity, Volume, Variety) as following challenges that address RQ4: *what are the main future challenges?*.

As a matter of fact, and as shown in Section 4, the necessity of dealing with fast growing (velocity), memory-intensive (volume), high-dimensionality (variety) datasets is fostering the adoption of advanced ML approaches to solve the problem of L-PBF data processing [18,144]. In this context, data-driven techniques such as supervised, unsupervised and reinforcement learning, are progressively assuming greater significance in in-situ monitoring and process control tasks [18,142,143].

6.1. Velocity challenge

Regardless of the type of sensor used, online control requires that the sensors have a very fast response time and a high degree of spatial resolution [21]. Laser scanning speed in SLS/M are typically on the order of 100 to 1000 mm/s, while the laser focus area is on the order of 10–100 μm. Any electromagnetic monitoring system must be equally capable of reacting to these high scanning velocities and rapid melt pool dynamics in addition to being able to resolve slight spatial variations [145]. For

example, phenomena such as spatter, plume formation, laser modulation, and melt-pool oscillations may require data acquisition rates exceeding 10 kHz. These constraints lead to the utilization of relatively data-intensive, streaming imaging sensors in a real time monitoring and feedback control system [146].

While sensing techniques have achieved a high level of sampling rate and coverage for the majority of metal L-PBF process signatures (as reviewed in Section 4.2.1), the main challenge lies in the application of the data analysis methods within the context of ML or classical statistical approaches, especially in terms of real time defect detection computational speed. Another issue pertains to the speed of updating AM machine parameters.

6.2. Volume challenge

Due to the high frame rate requirements (e.g., ranging from a few to hundreds of kHz as shown in Table 5, Section 4.2.1), existing commercial in-situ monitoring systems result in the generation of enormous volumes of data (e.g., 100 GB for a 10 mm height cylindrical sample), which are very difficult to store and analyze up to the present date. For this reason, several authors propose data reduction techniques such as Principal Component Analysis (PCA) as a potential solution for managing heavy datasets [4,90].

Despite these efforts, there remain unresolved issues, specifically there is a lack of a common reference data structure, as well as of standard practices and unified systems for storing and handling information with a real big data approach [18]. This, added to the difficulty and costs related to data annotation, sets many challenges to the creation of suitable databases to train and validate ML algorithms. Research and standard bodies (e.g., ASTM, ISO, NIST) may address this issue in the interest of widespread market exploitation. A first step toward the development of a standard data-structure for AM processes, is the AM Material Database (AMMD) [151]. This is an open platform developed by the NIST, which provides a flexible data schema that is suitable for AM, included L-PBF, providing a reliable benchmark for the training and validation of ML algorithms.

6.3. Variety challenge

Using multiple sensor-based systems (i.e., sensor fusion [147]) to collect data from the manufacturing process is essential for better part quality monitoring and improving data collection capability. For example, a recent and promising paper illustrates a new technique that synchronizes high-speed XR imaging with high-speed IR imaging to L-PBF processes in real time and simultaneous observation of multiple phenomena (e.g., 3D melt pool visualization, vapor plume dynamics, spatter formation, thermal history, and point cooling rates) [148]. Other research is ongoing toward integrating new process sensors (e.g., accelerometers) and monitoring tools to allow for detailed characterization of the signatures [149], or integrating synchronized, in-situ acquisition of a thermal camera, high-speed visible camera, photodiode, and laser modulation signal during fabrication [146]. As an additional impetus to the sensor fusion approaches, this may lead to a hybridization with other traditional and non-traditional production processes, resulting in increased interest in data fusion [150].

7. Conclusion

This article suitable for expert and non-expert readers, introduces the AM technologies focusing on metal L-PBF. More in detail, SLS/M are the two processes on which online control is investigated following a structured framework. A comprehensive explanation of the production process is provided, encompassing the definition and review of the principal online controllable input parameters and observable output signatures. Additionally, this article reviews and discusses sensing techniques designed to capture signature signals from these types of processes. The state of the art on online feedback strategies is for closed loop control. Among these approaches, ML exhibit the highest potential for employing advanced techniques to tackle the three critical challenges associated with online control and big data framework (i.e., 3Vs: velocity, volume, and variety) in metal L-PBF. The developments and advancements in ML technologies are thoroughly reviewed, and prominent open challenges are identified and classified.

Declaration of competing interest

The authors report that there are no competing interests to declare.

Data availability

Data sharing is not applicable to this article as no new data were created or analyzed in this study.

References

[1] Wong KV, Hernandez A. A review of additive manufacturing. International Scholarly Research Network ISRN Mechanical Engineering 2012. https://doi.org/10.5402/2012/208760.
[2] Ghobakhloo M. Industry 4.0, digitization, and opportunities for sustainability. J Clean Prod 2020;252:119869. https://doi.org/10.1016/J.JCLEPRO.2019.119869. Apr.
[3] Calignano F, Galati M, Iuliano L. A metal powder bed fusion process in industry: qualification considerations. Machines 2019;7(4):72. https://doi.org/10.3390/MACHINES7040072.
[4] Grasso M, Colosimo BM. Process defects and in situ monitoring methods in metal powder bed fusion: a review. Meas Sci Technol Feb. 2017;28(4):044005. https://doi.org/10.1088/1361-6501/AA5C4F.
[5] Haleem A, Javaid M. Additive manufacturing applications in industry 4.0: a review. Journal of Industrial Integration and Management Oct. 2019;4(4):1930001. https://doi.org/10.1142/S2424862219300011.
[6] Zarrabeitia E, Bildosola I, Río Belver RM, Alvarez I, Cilleruelo-Carrasco E. Laser additive manufacturing: a patent overview. In: Engineering Digital Transformation: Proceedings of the 11th International Conference on Industrial Engineering and Industrial Management; 2019. p. 183–91. https://doi.org/10.1007/978-3-319-96005-0_23.
[7] Additive manufacturing trend report | Hubs. https://www.hubs.com/get/trends/. [Accessed 7 August 2021].
[8] Wohlers Report 2020. https://wohlersassociates.com/press83.html. [Accessed 7 August 2021].
[9] ISO/ASTM 52900:2015(en), additive manufacturing — general principles — terminology. https://www.iso.org/obp/ui/#iso:std:iso-astm:52900:ed-1:v1:en. [Accessed 7 August 2021].
[10] Gibson I, Rosen D, Stucker B, Khorasani M. Powder bed fusion. Additive Manufacturing Technologies 2021:125–70. https://doi.org/10.1007/978-3-030-56127-7_5.
[11] Mele M, Campana G, Monti GL. On the effect of irradiance on dimensional accuracy in multijet fusion additive manufacturing. Rapid Prototyp J 2021;27(6):1138–47. https://doi.org/10.1108/RPJ-07-2020-0180.
[12] Bhavar V, Kattire P, Patil V, Khot S, Gujar K, Singh R. A review on powder bed fusion technology of metal additive manufacturing. Additive Manufacturing Handbook May 2017:251–3. https://doi.org/10.1201/9781315119106-15.
[13] Bartlett JL, Li X. An overview of residual stresses in metal powder bed fusion. Addit Manuf May 2019;27:131–49. https://doi.org/10.1016/J.ADDMA.2019.02.020.
[14] Vlasea ML, Lane B, Lopez F, Mekhontsev S, Donmez A. Development of powder bed fusion additive manufacturing test bed for enhanced real-time process control. In: International Solid Freeform Fabrication Symposium; 2015.
[15] Wang Z, Pannier CP, Barton K, Hoelzle DJ. Application of robust monotonically convergent spatial iterative learning control to microscale additive manufacturing. Mechatronics Dec. 2018;56:157–65. https://doi.org/10.1016/J.MECHATRONICS.2018.09.003.
[16] Scime L, Beuth J. Anomaly detection and classification in a laser powder bed additive manufacturing process using a trained computer vision algorithm. Addit Manuf Jan. 2018;19:114–26. https://doi.org/10.1016/J.ADDMA.2017.11.009.
[17] Mani M, Lane BM, Donmez MA, Feng SC, Moylan SP. A review on measurement science needs for real-time control of additive manufacturing metal powder bed fusion processes. International Journal of Production Research Mar. 2016;55(5):1400–18. https://doi.org/10.1080/00207543.2016.1223378.
[18] Di Cataldo S, Vinco S, Urgese G, Calignano F, Ficarra E, Macii A, et al. Optimizing quality inspection and control in powder bed metal additive manufacturing: challenges and research directions. Proc IEEE Apr. 2021;109(4):326–46. https://doi.org/10.1109/JPROC.2021.3054628.
[19] Moen R, Norman C. The History of the PDCA Cycle. Tokyo: Congress; 2009.
[20] Pittaway L, Robertson M, Munir K, Denyer D, Neely A. Networking and innovation: a systematic review of the evidence. International Journal of

Management Reviews Sep. 2004;5–6(3–4):137–68. https://doi.org/10.1111/J.1460-8545.2004.00101.X.
[21] McCann R, Obeidi MA, Hughes C, McCarthy É, Egan DS, Vijayaraghavan RK, et al. In-situ sensing, process monitoring and machine control in laser powder bed fusion: a review. Addit Manuf Sep. 2021;45:102058. https://doi.org/10.1016/J.ADDMA.2021.102058.
[22] Spears TG, Gold SA. In-process sensing in selective laser melting (SLM) additive manufacturing. Integrating Materials and Manufacturing Innovation 2016 5:1 Feb. 2016;5(1):16–40. https://doi.org/10.1186/S40192-016-0045-4.
[23] Chua ZY, Ahn IH, Moon SK. Process monitoring and inspection systems in metal additive manufacturing: status and applications. International Journal of Precision Engineering and Manufacturing - Green Technology Apr. 2017;4(2):235–45. https://doi.org/10.1007/S40684-017-0029-7.
[24] Taherkhani K, Ero O, Liravi F, Toorandaz S, Toyserkani E. On the application of in-situ monitoring systems and machine learning algorithms for developing quality assurance platforms in laser powder bed fusion: a review. J Manuf Process Aug. 2023;99:848–97. https://doi.org/10.1016/J.JMAPRO.2023.05.048.
[25] Herzog T, Brandt M, Trinchi A, Sola A, Molotnikov A. Process monitoring and machine learning for defect detection in laser-based metal additive manufacturing. J Intell Manuf 2023. https://doi.org/10.1007/S10845-023-02119-Y.
[26] Zorriassatine F, Tannock JDT. A review of neural networks for statistical process control. J Intell Manuf 1998;9(3):209–24. https://doi.org/10.1023/A:1008818817588.
[27] Lanzetta M, Santochi M, Tantussi G. On-line control of robotized gas metal arc welding. CIRP Annals Jan. 2001;50(1):13–6. https://doi.org/10.1016/S0007-8506(07)62060-5.
[28] Dalpadulo E, Pini F, Leali F. Integrated CAD platform approach for Design for Additive Manufacturing of high performance automotive components. International Journal on Interactive Design and Manufacturing (IJIDeM) 2020 14:3 Aug. 2020;14(3):899–909. https://doi.org/10.1007/S12008-020-00684-7.
[29] Lupi F, Rowley S, Chyba M, Lanzetta M. Reconstruction of tubular structures from 2.5 D point clouds: a mesophotic gorgonian coral case study. ANZIAM J 2021;63:C1–14. https://doi.org/10.21914/anziamj.v63.17151.
[30] Grimm T. User's guide to rapid prototyping. Society of Manufacturing Engineers 2004.
[31] Brown AC, De Beer D. Development of a stereolithography (STL) slicing and G-code generation algorithm for an entry level 3-D printer. IEEE AFRICON Conference 2013. https://doi.org/10.1109/AFRCON.2013.6757836.
[32] Lupi F, Cimino MGCA, Berlec T, Galatolo FA, Corn M, Rožman N, Rossi A, Lanzetta M. Blockchain-based shared additive manufacturing. Comput Ind Eng Jul 2023:109497. https://doi.org/10.1016/J.CIE.2023.109497.
[33] Rahman Chukkan J, Vasudevan M, Muthukumaran S, Ravi Kumar R, Chandrasekhar N. Simulation of laser butt welding of AISI 316L stainless steel sheet using various heat sources and experimental validation. J Mater Process Technol May 2015;219:48–59. https://doi.org/10.1016/J.JMATPROTEC.2014.12.008.
[34] Kuryntsev SV, Morushkin AE, Gilmutdinov AK. Fiber laser welding of austenitic steel and commercially pure copper butt joint. Opt Lasers Eng Mar. 2017;90:101–9. https://doi.org/10.1016/J.OPTLASENG.2016.10.008.
[35] Steen WM, Mazumder J. Laser material processing. In: Springer Science & Business Media; 2010.
[36] Prokhorov AM, Konov VI, Ursu I, Mihailescu IN. Laser heating of metals. Laser Heating of Metals Jan. 2018:1–239. https://doi.org/10.1201/9781351073943.
[37] Niu Y, Wang Y, Liu X, Zhang C, Zhu S. Laser beam quality factor M2 and its measurement. Laser Processing of Materials and Industrial Applications II Aug. 1998;3550:378–82. https://doi.org/10.1117/12.317915.
[38] Singh R, Gupta A, Tripathi O, Srivastava S, Singh B, Awasthi A, et al. Powder bed fusion process in additive manufacturing: an overview. Mater Today Proc Jan. 2020;26:3058–70. https://doi.org/10.1016/J.MATPR.2020.02.635.
[39] Prashanth H Attar KG, Zhang L-C, Calin M, Okulov IV, Scudino S, Yang C, et al. Effect of powder particle shape on the properties of in situ Ti–TiB composite materials produced by selective laser melting. J Mater Sci Technol Oct. 2015;31(10):1001–5. https://doi.org/10.1016/J.JMST.2015.08.007.
[40] Ferrar B, Mullen L, Jones E, Stamp R, Sutcliffe CJ. Gas flow effects on selective laser melting (SLM) manufacturing performance. J Mater Process Technol Feb. 2012;212(2):355–64. https://doi.org/10.1016/J.JMATPROTEC.2011.09.020.
[41] Amado A, Schmid M, Levy G, Wegener K. Advances in SLS powder characterization. International Solid Freeform Fabrication Symposium; 2011.
[42] Tapia G, Elwany A. A review on process monitoring and control in metal-based additive manufacturing. J Manuf Sci Eng Dec. 2014;136(6). https://doi.org/10.1115/1.4028540.
[43] ISO - ISO 9001:2015 - Quality management systems — Requirements. https://www.iso.org/standard/62085.html. [Accessed 7 August 2021].
[44] Wang C, Tan XP, Tor SB, Lim CS. Machine learning in additive manufacturing: state-of-the-art and perspectives. Addit Manuf Dec. 2020;36:101538. https://doi.org/10.1016/J.ADDMA.2020.101538.
[45] Reiff C, Wulle F, Riedel O. On inline process control for selective laser sintering. In: Proceedings of the 8th International Conference on Mass Customization and Personalization. 23, no. 6; 2014. p. 230.
[46] Calignano F, Lorusso M, Pakkanen J, Trevisan F, Ambrosio EP, Manfredi D, et al. Investigation of accuracy and dimensional limits of part produced in aluminum alloy by selective laser melting. The International Journal of Advanced Manufacturing Technology 2017;88:451–8.
[47] Salarian M, Toyserkani E. The use of nano-computed tomography (nano-CT) in non-destructive testing of metallic parts made by laser powder-bed fusion additive manufacturing. The International Journal of Advanced Manufacturing Technology 2018 98:9 Jul. 2018;98(9):3147–53. https://doi.org/10.1007/S00170-018-2421-Z.
[48] Aloini D, Dulmin R, Mininno V, Stefanini A, P. Z.- Sustainability, and undefined 2020. Driving the transition to a circular economic model: a systematic review on drivers and critical success factors in circular economy. Sustainability 2020;12(24):10672. https://doi.org/10.3390/su122410672.
[49] Scopus preview - Scopus - Welcome to Scopus. https://www.scopus.com/home.uri. [Accessed 7 August 2021].
[50] Falagas ME, Pitsouni EI, Malietzis GA, Pappas G. Comparison of PubMed, Scopus, web of science, and Google scholar: strengths and weaknesses. Wiley Online Library Feb. 2008;22(2):338–42. https://doi.org/10.1096/fj.07-9492LSF.
[51] Lupi F, Lanzetta M. A Novel Approach for Cooperative Scientific Literature Search and Socialization1542. *Springer*; 2022. p. 31–45. https://doi.org/10.1007/978-3-030-96060-5_3. CCIS.
[52] Hojjatzadeh SMH, Guo Q, Parab ND, Qu M, Escano LI, Fezzaa K, et al. In-situ characterization of pore formation dynamics in pulsed wave laser powder bed fusion. Materials 2021;14(11):2936. https://doi.org/10.3390/ma14112936.
[53] Evans R, Walker J, Middendorf J, Gockel J. Modeling and monitoring of the effect of scan strategy on microstructure in additive manufacturing. Metall Mater Trans A Phys Metall Mater Sci Aug. 2020;51(8):4123–9. https://doi.org/10.1007/S11661-020-05830-0.
[54] Modaresialam M, Roozbahani H, Alizadeh M, Salminen A, Handroos H. In-situ monitoring and defect detection of selective laser melting process and impact of process parameters on the quality of fabricated SS 316L. ieeeAccess 2022;10:46100–13. https://doi.org/10.1109/ACCESS.2022.3169509.
[55] Yuasa K, Tagami M, Yonehara M, Ikeshoji TT, Takeshita K, Aoki H, et al. Influences of powder characteristics and recoating conditions on surface morphology of powder bed in metal additive manufacturing. The International Journal of Advanced Manufacturing Technology 2021 115:11 Jun. 2021;115(11):3919–32. https://doi.org/10.1007/S00170-021-07359-X.
[56] Dadbakhsh S, Mertens R, Hao L, Van Humbeeck J, Kruth J-P. Selective laser melting to manufacture 'in situ' metal matrix composites: a review. Wiley Online Library Mar. 2019;21(3). https://doi.org/10.1002/adem.201801244.
[57] Höfflin D, Rosilius M, Seitz P, Schiffler A, Hartmann J. Opto-thermal investigation of additively manufactured steel samples as a function of the hatch distance. Sensors 2021;22(1):46. https://doi.org/10.3390/s22010046.
[58] Downing D, Miller J, McMillan M, Leary M, Wischeropp T, Emmelmann C, et al. The effect of geometry on local processing state in additively manufactured Ti-6Al-4V lattices. Integr Mater Manuf Innov Sep. 2021;10(3):508–23. https://doi.org/10.1007/S40192-021-00225-4.
[59] Klingaa CG, Mohanty S, Funch CV, Hjermitslev AB, Haahr-Lillevang L, Hattel JH. Towards a digital twin of laser powder bed fusion with a focus on gas flow variables. Journal of Manufacturing Processes 2021;65:312–27. https://doi.org/10.1016/j.jmapro.2021.03.035.
[60] Mahmoudi M, Tapia G, Karayagiz K, Franco B, Ma J, Arroyave R, et al. Multivariate calibration and experimental validation of a 3D finite element thermal model for laser powder bed fusion metal additive manufacturing. Integr Mater Manuf Innov, Sep 2018;7:116–35. https://doi.org/10.1007/s40192-018-0113-z.
[61] Bisht M, Ray N, Verbist F, Coeck S. Correlation of selective laser melting-melt pool events with the tensile properties of Ti-6Al-4V ELI processed by laser powder bed fusion. Addit Manuf 2018;22:302–6. https://doi.org/10.1016/j.addma.2018.05.004.
[62] Lane B, Zhirnov I, Mekhontsev S, Grantham S, Ricker R, Rauniyar S, et al. Transient laser energy absorption, co-axial melt pool monitoring, and relationship to melt pool morphology. *Elsevier*, Additive Manufacturing 2021;36:101504. https://doi.org/10.1016/j.addma.2020.101504.
[63] Simonds B, Tanner J, Artusio-Glimps A, Williams PA, Parab N, Zhao C, et al. The causal relationship between melt pool geometry and energy absorption measured in real time during laser-based manufacturing. Elsevier, Materials today June 2021;23:101049. https://doi.org/10.1016/j.apmt.2021.101049.
[64] Cheng B, Lydon J, Cooper K, Cole V, Northrop P, Chou K. Melt pool sensing and size analysis in laser powder-bed metal additive manufacturing. Journal of Manufacturing Processes 2018;32:744–53. https://doi.org/10.1016/j.jmapro.2018.04.002.
[65] Chen Z, Zong X, Shi J, Zhang X. Online monitoring based on temperature field features and prediction model for selective laser sintering process. Applied sciences 2018;8(12):2383. https://doi.org/10.3390/app8122383.
[66] Jeronen J, Tuovinen T, Kurki M. One-dimensional thermomechanical model for additive manufacturing using laser-based powder bed fusion. Computation May 2022;10(6):83. https://doi.org/10.3390/computation10060083.
[67] Chen X Duan X, Zhu K, Long T, Huang S, Jerry FYH. The Thermo-mechanical coupling effect in selective laser melting of aluminum alloy powder. Materials 2021;14(7):1673. https://doi.org/10.3390/ma14071673.
[68] Fisher BA, Lane B, Yeung H, Beuth J. Toward determining melt pool quality metrics via coaxial monitoring in laser powder bed fusion. Manufacturing Letters 2018;15:119–21. https://doi.org/10.1016/j.mfglet.2018.02.009.
[69] Grasso M, Colosimo BM. A statistical learning method for image-based monitoring of the plume signature in laser powder bed fusion. Robot Comput Integr Manuf Jun. 2019;57:103–15. https://doi.org/10.1016/J.RCIM.2018.11.007.
[70] Malekipour E, El-Mounayri H. Common defects and contributing parameters in powder bed fusion AM process and their classification for online monitoring and control: a review. The International Journal of Advanced Manufacturing

Technology 2017 95:1 Oct. 2017;95(1):527–50. https://doi.org/10.1007/S00170-017-1172-6.
[71] Ulbricht A, Mohr G, Altenburg SJ, Oster S, Maierhofer C, Bruno G. Can potential defects in LPBF be healed from the laser exposure of subsequent layers? A quantitative study. Metals 2021 Jun. 2021;11(7):1012. https://doi.org/10.3390/MET11071012.
[72] Minet K, Saharan A, Loesser A, Raitanen N. Superalloys, powders, process monitoring in additive manufacturing. Additive Manufacturing for the Aerospace Industry 2019:163–85.
[73] Coeck S, Bisht M, Plas J, Verbist F. Prediction of lack of fusion porosity in selective laser melting based on melt pool monitoring data. Addit Manuf 2019;25:347–56. https://doi.org/10.1016/j.addma.2018.11.015.
[74] Li J, Cao L, Xu J, Wang S, Zhou Q. In situ porosity intelligent classification of selective laser melting based on coaxial monitoring and image processing. Measurement 2022;187:110232. https://doi.org/10.1016/j.measurement.2021.110232.
[75] Wang P, Yang Y, Moghaddam NS. Process modeling in laser powder bed fusion towards defect detection and quality control via machine learning: the state-of-the-art and research challenges. Journal of Manufacturing Processes 2022;73:961–84. https://doi.org/10.1016/j.jmapro.2021.11.037.
[76] Fang ZC, Wu ZL, Huang CG, Wu CW. Micro-scale thermodynamic model of microstructure and stress evolution in parts via selective laser melting. J Mater Sci Jul 2022;57(25):11918–33. https://doi.org/10.1007/S10853-022-07046-6.
[77] Fischer T, Kuhn B, Rieck D, Schulz A, Trieglaff R, Wilms MB. Fatigue cracking of additively manufactured materials—process and material perspectives. Applied Sciences 2020;10(16):5556. https://doi.org/10.3390/app10165556.
[78] Zhang J, Wu J, Zhao X, Yuan S, Ma G, Li J, et al. Laser ultrasonic imaging for defect detection on metal additive manufacturing components with rough surfaces. Appl Opt 2020;59(33):10380–8. https://doi.org/10.1364/AO.405284.
[79] Repossini G, Laguzza V, Grasso M, Colosimo BM. On the use of spatter signature for in-situ monitoring of laser powder bed fusion. Addit Manuf Aug. 2017;16:35–48. https://doi.org/10.1016/J.ADDMA.2017.05.004.
[80] Liu J, Wen P. Metal vaporization and its influence during laser powder bed fusion process. Materials & Design 2022;215:110505. https://doi.org/10.1016/j.matdes.2022.110505.
[81] Kim F, Garboczi EJ. Characterizing the effects of laser control in laser powder bed fusion on near-surface pore formation via combined analysis of in-situ melt pool monitoring and X-ray computed tomography. Addit Manuf 2021;48:102372. https://doi.org/10.1016/j.addma.2021.102372.
[82] Li C, Liu ZY, Fang XY, Guo YB. Residual stress in metal additive manufacturing. Procedia Cirp 2018;71:348–53. https://doi.org/10.1016/j.procir.2018.05.039.
[83] Grasso M, Remani A, Dickins A, Colosimo BM, Leach RK. In-situ measurement and monitoring methods for metal powder bed fusion: an updated review. Meas Sci Technol Jul. 2021;32(11):112001. https://doi.org/10.1088/1361-6501/AC0B6B.
[84] Wang D, Chen P, Pan R, Zha C, Fan J, Kong S, Li N, et al. Research on in situ monitoring of selective laser melting: a state of the art review. Int J Adv Manuf Technol Apr. 2021;113(11–12):3121–38. https://doi.org/10.1007/S00170-020-06432-1.
[85] Zhao C, Fezzaa K, Cunningham RW, Wen H, De Carlo F, Chen L, et al. Real-time monitoring of laser powder bed fusion process using high-speed X-ray imaging and diffraction. Scientific Reports 2017 7:1 Jun. 2017;7(1):1–11. https://doi.org/10.1038/s41598-017-03761-2.
[86] Bidare P, Maier RRJ, Beck RJ, Shephard JD, Moore AJ. An open-architecture metal powder bed fusion system for in-situ process measurements. Addit Manuf Aug. 2017;16:177–85. https://doi.org/10.1016/J.ADDMA.2017.06.007.
[87] Bitharas I, Parab N, Zhao C, Sun T, Rollett AD, Moore AJ. The interplay between vapour, liquid, and solid phases in laser powder bed fusion. Nat Commun 2022;13(1):2959. https://doi.org/10.1038/s41467-022-30667-z.
[88] Ji B Wu X, Zhou J, Yang H, Peng D, Wang Z, Wu Y, et al. In situ monitoring methods for selective laser melting additive manufacturing process based on images — a review. China Foundry Jul. 2021;18(4):265–85. https://doi.org/10.1007/S41230-021-1111-X.
[89] Alkahari M, Furumoto T, Ueda T, Hosokawa A. Consolidation characteristics of ferrous-based metal powder in additive manufacturing. Journal of Advanced Mechanical Design, Systems, and Manufacturing 2023;8(1):JAMDSM0009-JAMDSM0009. https://doi.org/10.1299/jamdsm.2014jamdsm0009.
[90] Colosimo BM, Grasso M. Spatially weighted PCA for monitoring video image data with application to additive manufacturing. J Qual Technol 2018;50(4):391–417. https://doi.org/10.1080/00224065.2018.1507563.
[91] Yang L, Lo L, Ding S, Özel T. Monitoring and detection of meltpool and spatter regions in laser powder bed fusion of super alloy Inconel 625. Progress in Additive Manufacturing Dec. 2020;5(4):367–78. https://doi.org/10.1007/S40964-020-00140-8.
[92] Vasileska E, Demir AG, Colosimo BM, Previtali B. Layer-wise control of selective laser melting by means of inline melt pool area measurements. J Laser Appl May 2020;32(2):022057. https://doi.org/10.2351/7.0000108.
[93] Scime L, Fisher B, Beuth J. Using coordinate transforms to improve the utility of a fixed field of view high speed camera for additive manufacturing applications. Manuf Lett Jan. 2018;15:104–6. https://doi.org/10.1016/J.MFGLET.2018.01.006.
[94] Aminzadeh M, Kurfess TR. Online quality inspection using Bayesian classification in powder-bed additive manufacturing from high-resolution visual camera images. J Intell Manuf Aug. 2019;30(6):2505–23. https://doi.org/10.1007/S10845-018-1412-0.
[95] Knaak C, Masseling L, Duong E, Abels P, Gillner A. Improving build quality in laser powder bed fusion using high dynamic range imaging and model-based reinforcement learning. IEEE Access 2021;9:55214–31. https://doi.org/10.1109/ACCESS.2021.3067302.
[96] Li J, Zhou Q, Huang X, Li M, Cao L. In situ quality inspection with layer-wise visual images based on deep transfer learning during selective laser melting. J Intell Manuf 2021:1–15. https://doi.org/10.1007/S10845-021-01829-5.
[97] Lin Z, Lai Y, Pan T, Zhang W, Zheng J, Ge X, et al. A new method for automatic detection of defects in selective laser melting based on machine vision. Materials 2021;14(15):4175. https://doi.org/10.3390/ma14154175.
[98] Cannizzaro D, Varrella AG, Paradiso S, Sampieri R, Chen Y, Macii A, et al. In-situ defect detection of metal additive manufacturing: an integrated framework. IEEE Transactions on Emerging Topics in Computing 2021;10(1):74–86. https://doi.org/10.1109/TETC.2021.3108844.
[99] Bugatti M, Colosimo BM. Towards real-time in-situ monitoring of hot-spot defects in L-PBF: a new classification-based method for fast video-imaging data analysis. J Intell Manuf Jan. 2022;33(1):293–309. https://doi.org/10.1007/S10845-021-01787-Y.
[100] Gaikwad A, Imani F, Yang H, Reutzel E, Rao P. In situ monitoring of thin-wall build quality in laser powder bed fusion using deep learning. Smart and Sustainable Manufacturing Systems 2019;(3)1. doi:10.1520/SSMS20190027.
[101] Akhil V, Raghav G, Arunachalam N, Srinivas DS. Image data-based surface texture characterization and prediction using machine learning approaches for additive manufacturing. Journal of Computing and Information Science in Engineering 2020;20(2):021010. https://doi.org/10.1115/1.4045719.
[102] Ansari MA, Crampton A, Garrard R, Cai B, Attallah M. A convolutional neural network (CNN) classification to identify the presence of pores in powder bed fusion images. Int J Adv Manuf Technol Jun. 2022;120(7–8):5133–50. https://doi.org/10.1007/S00170-022-08995-7.
[103] Caggiano A, Zhang J, Alfieri V, Caiazzo F, Gao R, Teti R. Machine learning-based image processing for on-line defect recognition in additive manufacturing. CIRP annals 2019;68(1):451–4. https://doi.org/10.1016/j.cirp.2019.03.021.
[104] Yazdi R, Imani F, Yang H. A hybrid deep learning model of process-build interactions in additive manufacturing. J Manuf Syst 2020;57:460–8. https://doi.org/10.1016/j.jmsy.2020.11.001.
[105] Yadav P, Joffre T, Rigo O, Arvieu C, Le Guen E, Lacoste E. Inline drift detection using monitoring systems and machine learning in selective laser melting. Wiley Online Library Dec. 2020;22(12). https://doi.org/10.1002/adem.202000660.
[106] Barrett C, Carradero C, Harris E, Rogers K, MacDonald E, Conner B. Statistical analysis of spatter velocity with high-speed stereovision in laser powder bed fusion. Progress in Additive Manufacturing Dec. 2019;4(4):423–30. https://doi.org/10.1007/S40964-019-00094-6.
[107] Wang Z, Wang X, Zhou X, Ye G, Cheng X, Zhang P. Investigation into spatter particles and their effect on the formation quality during selective laser melting processes. Computer Modeling in Engineering & Sciences Jun. 2020;124(1):243. https://doi.org/10.32604/CMES.2020.09934.
[108] Lu Q, Nguyen N, Hum A, Tran T, Wong CH. Optical in-situ monitoring and correlation of density and mechanical properties of stainless steel parts produced by selective laser melting process based on varied energy density. J Mater Process Technol 2019;271:520–31. https://doi.org/10.1016/j.jmatprotec.2019.04.026.
[109] Yan H, Grasso M, Paynabar K, Colosimo BM. Real-time detection of clustered events in video-imaging data with applications to additive manufacturing. IISE Trans 2022;54(5):464–80. https://doi.org/10.1080/24725854.2021.1882013.
[110] Kalms M, Narita R, Thomy C, Vollertsen F, Bergmann RB. New approach to evaluate 3D laser printed parts in powder bed fusion-based additive manufacturing in-line within closed space. Addit Manuf 2019;26:161–5. https://doi.org/10.1016/j.addma.2019.01.011.
[111] Chen Z, Zong X, Zhang X. Analysis of the temperature field during the selective laser melting process based on a finite element model. International Journal of Manufacturing Research 2019;14(4):355–72. https://doi.org/10.1504/IJMR.2019.104399.
[112] Bartlett J, Heim F, Murty Y, Li X. In situ defect detection in selective laser melting via full-field infrared thermography. Addit Manuf 2018;24:595–605. https://doi.org/10.1016/j.addma.2018.10.045.
[113] Mahmoudi M, Ezzat AA, Elwany A. Layerwise anomaly detection in laser powder-bed fusion metal additive manufacturing. J Manuf Sci Eng 2019;141(3):031002. https://doi.org/10.1115/1.4042108.
[114] Mitchell J, Ivanoff T, Dagel D, Madison JD, Jared B. Linking pyrometry to porosity in additively manufactured metals. Addit Manuf 2020;31:100946. https://doi.org/10.1016/j.addma.2019.100946.
[115] Mahato V, Obeidi MA, Brabazon D, Cunningham P. Detecting voids in 3D printing using melt pool time series data. J Intell Manuf Mar. 2022;33(3):845–52. https://doi.org/10.1007/S10845-020-01694-8.
[116] Baumgartl H, Tomas J, Buettner R, Merkel M. A deep learning-based model for defect detection in laser-powder bed fusion using in-situ thermographic monitoring. Progress in Additive Manufacturing Sep. 2020;5(3):277–85. https://doi.org/10.1007/S40964-019-00108-3.
[117] Cheng B, Lydon J, Cooper K, Cole V, Northrop P, Chou K. Melt pool sensing and size analysis in laser powder-bed metal additive manufacturing. Journal of Manufacturing Processes 2018;32:744–53. https://doi.org/10.1016/j.jmapro.2018.04.002.
[118] Grasso M, Demir A, Previtali B, Colosimo BM. In situ monitoring of selective laser melting of zinc powder via infrared imaging of the process plume. Robotics and Computer-Integrated Manufacturing 2018;49:229–39. https://doi.org/10.1016/j.rcim.2017.07.001.

[119] Tsiamyrtzis P, Grasso MLG, Colosimo BM. Image based statistical process monitoring via partial first order stochastic dominance. Qual Eng 2022;34(1):96–124. https://doi.org/10.1080/08982112.2021.2008974.
[120] Lough C, Wang X, Smith C, Landers RG, Bristow DA, Drallmeier JA, et al. Correlation of SWIR imaging with LPBF 304L stainless steel part properties. Addit Manuf 2020;35:101359. https://doi.org/10.1016/j.addma.2020.101359.
[121] Lough C, Liu T, Wang X, Brown B, Robert G, Bristow AD, et al. Local prediction of laser powder bed fusion porosity by short-wave infrared imaging thermal feature porosity probability maps. J Mater Process Technol April 2022;302:117473. https://doi.org/10.1016/j.jmatprotec.2021.117473.
[122] Ma H, Mao Z, Feng W, Yang Y, Hao C, Zhou J, et al. Online in-situ monitoring of melt pool characteristic based on a single high-speed camera in laser powder bed fusion process. Appl Therm Eng 2022;211:118515. https://doi.org/10.1016/j.applthermaleng.2022.118515.
[123] Oster S, Fritsch T, Ulbricht A, Mohr G, Bruno G, Maierhofer C, Altenburg SJ. On the registration of thermographic in situ monitoring data and computed tomography reference data in the scope of defect prediction in laser powder bed fusion. Metals 2022;12(6):947. https://doi.org/10.3390/met12060947.
[124] Wimmer A, Hofstaetter F, Jugert C, Wudy K, Zaeh MF. In situ alloying: investigation of the melt pool stability during powder bed fusion of metals using a laser beam in a novel experimental set-up. Progress in Additive Manufacturing Apr. 2022;7(2):351–9. https://doi.org/10.1007/S40964-021-00233-Y.
[125] Lough C, Escano LI, Qu M, Smith CC, Landers RG, Bristow DA, et al. In-situ optical emission spectroscopy of selective laser melting. Journal of Manufacturing Processes 2020;53:336–41. https://doi.org/10.1016/j.jmapro.2020.02.016.
[126] Montazeri M, Nassar AR, Dunbar AJ, Rao P. In-process monitoring of porosity in additive manufacturing using optical emission spectroscopy. IISE Trans May 2020;52(5):500–15. https://doi.org/10.1080/24725854.2019.1659525.
[127] Gerdes N, Hoff C, Hermsdorf J, Kaierle S, Overmeyer L. Hyperspectral imaging for prediction of surface roughness in laser powder bed fusion. Int J Adv Manuf Technol Jul. 2021;115(4):1249–58. https://doi.org/10.1007/S00170-021-07274-1.
[128] Everton S, Dickens P, Tuck C, Dutton B. Using laser ultrasound to detect subsurface defects in metal laser powder bed fusion components. JOM Mar. 2018;70(3):378–83. https://doi.org/10.1007/S11837-017-2661-7.
[129] Kouprianoff D. Investigation of acoustic emission signal during laser powder bed fusion at different operating modes. South African Journal of Industrial Engineering 2021;32(3):279–83. https://doi.org/10.7166/32-3-2663.
[130] Luo S, Ma X, Xu J, Li M, Cao L. Deep learning based monitoring of spatter behavior by the acoustic signal in selective laser melting. Sensors 2021;21(21):7179. https://doi.org/10.3390/s21217179.
[131] Yang T, Jin Y, Squires B, Choi TY, Dahotre NB, Neogi A. In-situ monitoring and ex-situ elasticity mapping of laser-induced metal melting pool using ultrasound: numerical and experimental approaches. Journal of Manufacturing Processes 2021;71:178–86. https://doi.org/10.1016/j.jmapro.2021.08.031.
[132] Pandiyan V, Drissi-Daoudi R, Shevchik S, Masinelli G, Le-Quang T, Loge R, et al. Deep transfer learning of additive manufacturing mechanisms across materials in metal-based laser powder bed fusion process. J Mater Process Technol 2022;303:117531. https://doi.org/10.1016/j.jmatprotec.2022.117531.
[133] Chivel Y, Smurov I. On-line temperature monitoring in selective laser sintering/melting. Physics Procedia 2010;5:515–21. https://doi.org/10.1016/j.phpro.2010.08.079.
[134] Bayle F, Doubenskaia M. Selective laser melting process monitoring with high speed infra-red camera and pyrometer. Fundamentals of laser assisted micro-and nanotechnologies. SPIE 2008, January;6985:39–46. https://doi.org/10.1117/12.786940.
[135] Slotwinski J, Garboczi EJ. Porosity of additive manufacturing parts for process monitoring. In: AIP conference proceedings, 1581, no. 1. American Institute of Physics; 2014, February. p. 1197–204. https://doi.org/10.1063/1.4864957.
[136] Yuan B, Giera B, Guss G, Matthews I, Mcmains S. In: Semi-supervised convolutional neural networks for in-situ video monitoring of selective laser melting. IEEE; 2019, January. p. 744–53. https://doi.org/10.1109/WACV.2019.00084.
[137] Rieder H, Dillhöfer A, Spies M, Bamberg J, Hess T. Ultrasonic online monitoring of additive manufacturing processes based on selective laser melting. In: AIP Conference Proceedings, 1650, no. 1. American Institute of Physics; 2015 March. p. 184–91. https://doi.org/10.1063/1.4914609.
[138] Fox JC, Lane BM, Yeung H. Measurement of process dynamics through coaxially aligned high speed near-infrared imaging in laser powder bed fusion additive manufacturing. Thermosense: thermal infrared applications XXXIX. In: SPIE. 10214; 2017. p. 34–50. https://doi.org/10.1117/12.2263863.
[139] Yeung H, Lane B, Fox J. Part geometry and conduction-based laser power control for powder bed fusion additive manufacturing. Addit Manuf Dec. 2019;30. https://doi.org/10.1016/J.ADDMA.2019.100844.
[140] Adnan M, Yang H, Kuo TH, Cheng FT, Tran HC. MPI-based system 2 for determining LPBF process control thresholds and parameters. IEEE Robotics and Automation Letters 2021;6(4):6553–60. https://doi.org/10.1109/LRA.2021.3092762.
[141] Xi Z. Model predictive control of melt pool size for the laser powder bed fusion process under process uncertainty. SCE-ASME Journal of Risk and Uncertainty in Engineering Systems, Part B: Mechanical Engineering 2022;8(1):011103. https://doi.org/10.1115/1.4051746.
[142] Sahar T, Rauf M, Murtaza A, Khan L, Ayub H, Jameel SM, et al. Anomaly detection in laser powder bed fusion using machine learning: a review. Results in Engineering March 2023;17:100803. https://doi.org/10.1016/j.rineng.2022.100803.
[143] Sing SL, Kuo CN, Shih CT, Ho CC, Chua CK. Perspectives of using machine learning in laser powder bed fusion for metal additive manufacturing. Virtual Phys Prototyp 2021;16(3):372–86. https://doi.org/10.1080/17452759.2021.1944229.
[144] Elambasseril J, Brandt M. Brandt M. Artificial intelligence: way forward to empower metal additive manufacturing product development–an overview, Materials Today. In: Proceedings. 58; 2022. p. 461–5. https://doi.org/10.1016/j.matpr.2022.02.485.
[145] Lott P, Schleifenbaum H, Meiners W, Wissenbach K, Hinke C, Bültmann J. Design of an optical system for the in situ process monitoring of selective laser melting (SLM). Phys Procedia Jan. 2011;12, no. PART 1:683–90. https://doi.org/10.1016/J.PHPRO.2011.03.085.
[146] Lane B, Whitenton E, Moylan S. Multiple sensor detection of process phenomena in laser powder bed fusion. Thermosense: Thermal Infrared Applications XXXVIII 2016;9861:20–8. https://doi.org/10.1117/12.2224390.
[147] Sasiadek JZ. Sensor fusion. Annu Rev Control Jan. 2002;26(2):203–28. https://doi.org/10.1016/S1367-5788(02)00045-7.
[148] Gould B, Wolff S, Parab N, Zhao C, Lorenzo-Martin MC, Fezzaa K, et al. In situ analysis of laser powder bed fusion using simultaneous high-speed infrared and X-ray imaging. JOM 2020 73:1 Jul. 2020;73(1):201–11. https://doi.org/10.1007/S11837-020-04291-5.
[149] Morante F, Palladino M, Lanzetta M. Towards an integrated sensor system for additive manufacturing. In: Industry 4.0 – Shaping The Future of The Digital World; Oct. 2020. p. 173–8. https://doi.org/10.1201/9780367823085-31.
[150] Rossi A, Lanzetta M. Integration of hybrid additive/subtractive manufacturing planning and scheduling by metaheuristics. Comput Ind Eng Jun. 2020;144. https://doi.org/10.1016/J.CIE.2020.106428.
[151] AM Material Database. https://ammd.nist.gov/. [Accessed 23 July 2022].